Lawrence Berkeley National Laboratory
Lawrence Berkeley National Laboratory

Title
RADIATION IMPEDANCE OF TORSIONALLY VIBRATING SEISMIC SOURCES

Permalink
https://escholarship.org/uc/item/6s40j1n3

Author
Dorn, Geoffrey A.

Publication Date
1981-03-01

eScholarship.org Powered by the California Digital Library
University of California

LBL-12335
Preprint

Lawrence Berkeley Laboratory
UNIVERSITY OF CALIFORNIA, BERKELEY

EARTH SCIENCES DIVISION

RECEIVED
LAWRENCE
BERKELEY LABORATORY
JUN 1 8
LIBRARY
AND
DOCUMENTS

Submitted to Geophysics

# RADIATION IMPEDANCE OF TORSIONALLY VIBRATING SEISMIC SOURCES

Geoffrey A. Dorn

March 1981

TWO-WEEK LOAN COPY

This is a Library Circulating Copy
which may be borrowed for two weeks.
For a personal retention copy, call
Tech. Info. Division, Ext. 6782

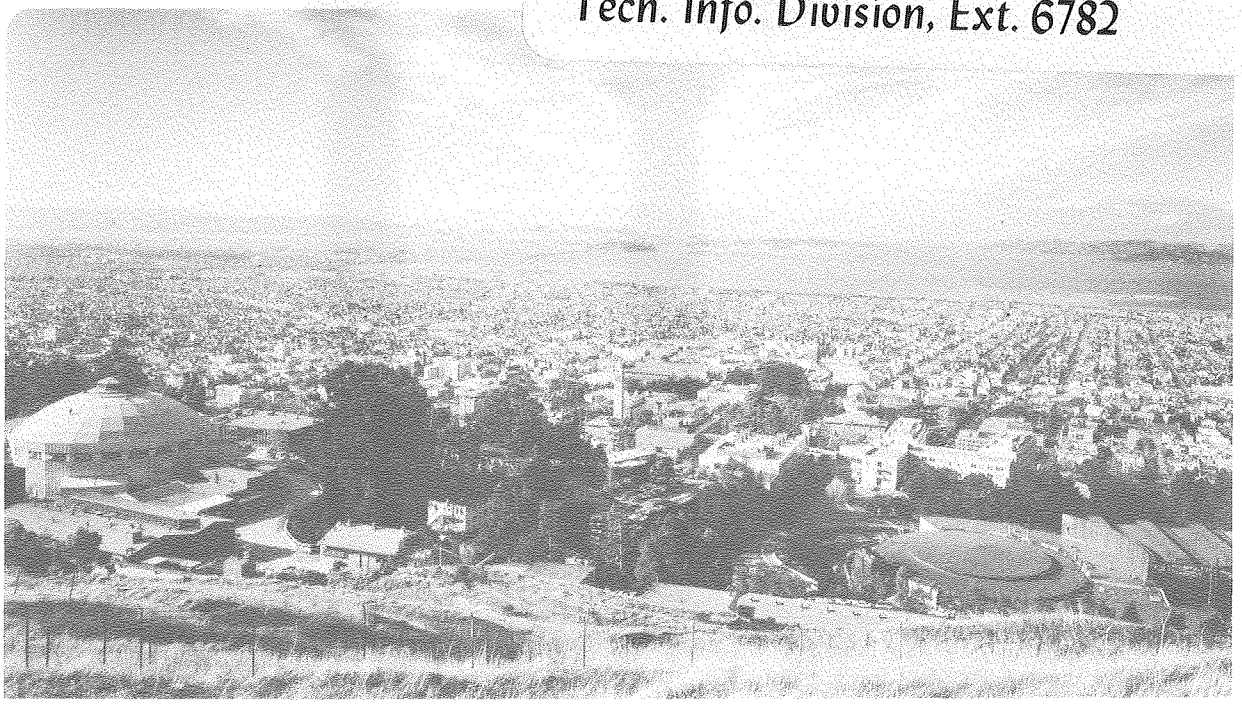

Prepared for the U.S. Department of Energy under Contract W-7405-ENG-48

LBL-12335
c.2

## DISCLAIMER

This document was prepared as an account of work sponsored by the United States Government. While this document is believed to contain correct information, neither the United States Government nor any agency thereof, nor the Regents of the University of California, nor any of their employees, makes any warranty, express or implied, or assumes any legal responsibility for the accuracy, completeness, or usefulness of any information, apparatus, product, or process disclosed, or represents that its use would not infringe privately owned rights. Reference herein to any specific commercial product, process, or service by its trade name, trademark, manufacturer, or otherwise, does not necessarily constitute or imply its endorsement, recommendation, or favoring by the United States Government or any agency thereof, or the Regents of the University of California. The views and opinions of authors expressed herein do not necessarily state or reflect those of the United States Government or any agency thereof or the Regents of the University of California.

*Submitted to GEOPHYSICS*

LBL-12335

# RADIATION IMPEDANCE OF TORSIONALLY VIBRATING SEISMIC SOURCES

Geoffrey A. Dorn
Engineering Geoscience
University of California
Earth Sciences Division
Lawrence Berkeley Laboratory
Berkeley, California 94720

March 1981

This work was supported by the Director, Office of Basic Energy Sciences, Division of Engineering, Mathematics, and Geosciences of the U. S. Department of Energy under contract no. W-7405-ENG-48.

# ABSTRACT

Theoretical modelling of the seismic radiation impedance for circular vibrator baseplates suggests methods in which impedance measurements might be used to determine the material properties of the medium below the baseplate. These studies also provide physical insight into the phenomena of vibrator - earth interraction.

The radiation impedance of a circular disk vibrating torsionally on an anelastic half-space has resonance peaks with a spacing that is a function of the ratio between baseplate radius and seismic wavelength. At low frequencies the shape of the impedance function is nearly independent of the source behavior, although the magnitude is affected. At high frequencies the impedance depends strongly on the flexibility of the baseplate. The mass of the baseplate introduces an additional resonant effect, the frequency of which is a function of the baseplate mass.

The presence of a surface layer produces an impedance curve which oscillates around the half-space response. The amplitude of the oscillations is a function of the acoustic impedance contrast and depends on the radiation pattern of the source. The oscillations are resonances caused by reflections within the surface layer, and both the period and amplitude of the oscillations are inversely proportional to the layer thickness. The amplitude of the layer resonance decreases rapidly as material damping increases.

With impedance measurements over a sufficiently broad frequency range, it may be feasable to use the half-space oscillations and the layer resonances to determine the shear velocity and thickness of the layer of material beneath the baseplate.

# I. INTRODUCTION

During the last two decades the vibrating seismic source or Vibroseis (a registered Trademark of the Continental Oil Co. Inc.) has become an increasingly important tool in land seismic exploration.A significant amount of progress has been made over that period of time in data collection, processing and analysis for vibrator surveys. There has been relatively little progress, however, toward understanding the interaction of vibrators and the earth.

In this paper the study of the radiation impedance function is used to develop an understanding of the interraction of a vibrator and the medium to which it is bonded in terms of physical phenomena occurring in the vicinity of the baseplate. From this analysis methods are suggested for using source related measurements to determine some physical parameters of the medium on which the vibrator rests.

The radiation impedance may be thought of as the load the vibrator experiences as it radiates energy into the medium. An analogy may be drawn between the radiation impedance and the impedance of an electric circuit. The circuit impedance, the load on the current source, is a function of the components in the circuit. The seismic radiation impedance, the load on the vibrator, depends on the components in its "circuit", which includes the baseplate and the medium on which it rests.

The impedance of a torsional source is considered in detail in this paper because such a vibrator on the surface of a plane-layered half-space produces only horizontally polarized ahear (SH) waves. As a result, the theory is somewhat simplified, and the impedance curves are simpler in form and more easily interpreted than those due to a vertical or horizontal vibrator. The observations made concerning the relationship between the vibrator impedance function and the properties of the medium can be extended to the vertical and horizontal impedance functions.

Most of the research on the impedance of a dynamically vibrating torsional source has been directed toward solving the mixed boundary value problem for a rigid source (displacement boundary condition at the source). Relatively little published literature is available on the solution of the simpler boundary value problem that involves a stress condition at the source.

The earliest solution for the radiation impedance of an oscillating rigid source was obtained by Sagoci (1944) using oblate spheroidal coordinates. He derived an exact solution in terms of infinite series of spheroidal functions. Although this solution is exact for a rigid baseplate on the surface of a half-space, it is numerically somewhat intractable.

Most of the research on torsional impedance functions between 1944 and 1970 was devoted to finding approximate solutions for thishalf-space problem appropriate for various ranges of frequency.

Collins (1962), Awojobi and Grootenhuis (1965) and Robertson (1967) each derived the same power series expansion for the problem of a rigid baseplate vibrating on the surface of an elastic half-space valid for low frequencies, using different methods. Robertson (1967) also suggested a method of obtaining the shear modulus of the elastic half-space using the impedance function. Stallybrass (1962, 1967) used variational techniques and asymptotic approximations to derive an expansion for the rigid source over a half-space valid at low frequencies, and a second expansion for high frequencies. Another high frequency solution has been presented by Thomas (1968).

Miller and Pursey (1954) have calculated the torsional radiation impedance at low frequencies for an elastic half-space with a stress distribution under the source which is proportional to radius (r). The impedance at low frequencies for a stress proportional to $r(1-r^2)^{\frac{1}{2}}$ has been calculated by Arnold et al. (1955) for a half-space, and by Bycroft (1956) for a half-space and an elastic stratum.

Several of the papers that contain solutions for the torsional source also present solutions for vertical and

horizontal vibrators (Miller and Pursey, 1954; Arnold et al., 1955; Bycroft, 1956; Awojobi and Grootenhuis, 1965). Although there appear to be no published radiation impedance calculations for a torsional vibrator over a layered medium, there have been several studies of the response of vertical and horizontal vibrators over layered media. Prominent among these are those by Luco (1974, 1976), Kashio (1970) and Wei (1971).

Since most research on radiation impedance functions has been directed toward determining the response of vibrating foundations, there has been little effort to interpret the response in terms of physical processes occuring in the medium (exceptions are the studies of Kashio, 1970, and Wei, 1971). Similarly there has been no extensive study of the effects of varying material properties or source parameters on the impedance.

The first step in calculating the radiation impedance is the solution of the elastodynamic wave equation. This equation is solved for the displacement at the surface of a plane-layered anealstic medium for an arbitrary torsional source. The torsional radiation impedance is then formulated in terms of this surface displacement and the stress beneath the baseplate

The majority of this paper is devoted to a parametric study of the torsional radiation impedance for half-space and layered models. The effects of changing material properties,

layer thickness and source type are analyzed in an effort to determine the physical phenomena giving rise to the effects and to obtain methods of deriving material properties from impedance measurements.

## THEORY

Consider the layered model and the circular cylindrical coordinate system shown in Figure 1. For a torsional vibrator, the radiation impedance is the total torque per unit area, divided by the mean angular velocity beneath the baseplate:

$$Z_T = \frac{\Gamma/\pi a^2}{i\omega(\overline{u/r})} \qquad (1)$$

where $(\overline{u/r})$ is the mean angular displacement under the baseplate. Assuming displacements are harmonic with time, $u(r,z,t)=u(r,z)e^{i\omega t}$, then $i\omega(\overline{u/r})$ is the mean angular velocity. The total torque is $\Gamma$, and a is the baseplate radius.

In order to calculate $Z_T$, the elastodynamic wave equation must be solved for the displacement produced by a torsional source at the surface of a plane-layered anelastic medium. In a source free region, this equation is:

$$\rho \frac{\partial^2 \vec{u}}{\partial t^2} = (\lambda+2\mu)\ \nabla\ (\nabla\cdot\vec{u}) - \mu\nabla\times\nabla\times\vec{u} \qquad (2)$$

For a torsional source in a plane layered medium, $u_r=u_z=0$, $\vec{u} = u_\phi\hat{\phi}$, and this equation reduces to a scalar differential equation in $u_\phi$:

$$\frac{\partial^2 u_\phi}{\partial z^2} + \frac{\partial}{\partial r}\left[\frac{1}{r}\frac{\partial(ru_\phi)}{\partial r}\right] + k_s^2 u_\phi = 0 \qquad (3)$$

where $k_s$ is the shear wave number. It is convenient to write equation (3) in a completely dimensionless form. Using the subscript o to indicate a dimensionless parameter, and scaling all distances to the baseplate radius, a, equation (3) becomes:

$$\frac{\partial^2 u_o}{\partial z_o^2} + \frac{\partial}{\partial r_o}\left(\frac{1}{r_o}\frac{\partial (r_o u_o)}{\partial r_o}\right) + k_{os}^2 u_o = 0 \qquad (4)$$

where $k_{os}=k_s a$ is the dimensionless shear wave number, and where the subscript $\phi$ has been dropped for convenience.

Applying a $J_1$ Hankel transform as defined in Table 1 to equation (4) reduces the problem to the solution of an ordinary differential equation:

$$\frac{\partial^2 \bar{u}_o}{\partial z_o^2} + (k_{os}^2 - \xi_o^2)\bar{u}_o = 0 \qquad (5)$$

where $\bar{u}_o$ is the transform of $u_o$ and $\xi_o$ is the transform variable.

In the mth layer of the N-layered medium shown in Figure 1 equation (5) has a solution of the form:

$$\bar{u}_{om} = A_{om} e^{-\beta_{om} z_{om}} + B_{om} e^{+\beta_{om} z_{om}} \qquad (6)$$

where:

$$\beta_{om} = (\xi_o^2 - k_{osm}^2)^{\frac{1}{2}}$$

At each interface in the layered medium, the displacement and stress are continuous:

$$u_{om}(r_o, h_{om}) = u_{om+1}(r_o, 0)$$

$$\mu_m \frac{\partial u_{om}(r_o, h_{om})}{\partial z_o} = \mu_{m+1} \frac{\partial u_{om+1}(r_o, 0)}{\partial z_o}$$

Applying the Hankel transform to these boundary conditions and substituting for the transformed displacement using equation (6), an expression may be derived for the ratio of the coefficients of the upgoing and downgoing waves in the mth layer:

$$\gamma_{om} \equiv \frac{B_{om}}{A_{om}} = \frac{\alpha_{om} + \kappa_{om}\, \gamma_{om+1}}{\kappa_{om} + \alpha_{om}\, \gamma_{om+1}}\, e^{-2\beta_{om}\, h_{om}} \qquad (7)$$

where:

$$\alpha_{om} = (1 - \varepsilon_{om+1})$$

$$\kappa_{om} = (1 + \varepsilon_{om+1})$$

$$\varepsilon_{om+1} = \frac{\mu_{m+1}\, \beta_{om+1}}{\mu_m\, \beta_{om}}$$

In an N-layered medium, where the Nth layer is the lower half-space, $\gamma_{oN} = 0$ because there is no upgoing wave in the lower half-space. Starting with $\gamma_{oN}$, the $\gamma_{oj}$, j = N-1, N-2, ... , 1 may be calculated recursively using equation (7).

In order to calculate $A_{o1}$ and $B_{o1}$ from $_{o1}$, the stress beneath the vibrator baseplate must be known. Two approaches may be taken to solve this problem. If the surface boundary

condition is specified in terms of the stress beneath the baseplate, the resulting boundary value problem may be solved by a straightforward application of transform techniques. If the source is defined by a displacement boundary condition at the surface, the resulting mixed boundary value problem must be solved for the stress beneath the source before the displacement can be calculated.

Once the stress under the baseplate is known, the solution for the displacement proceeds in the following manner. Suppose the stress distribution beneath the baseplate is some function f(r), known either analytically or numerically. Then the surface boundary condition in dimensionless form is:

$$\tau_{o\phi z}(r_o,0) = \begin{cases} P_o f_o(r_o) & r_o < 1 \\ 0 & r_o > 1 \end{cases} \qquad (8)$$

where $\tau_{o\phi z} = \tau_{\phi z}/\mu_1$, $f(r) = \mu_1 P_o f_o(r_o)$, $r_o = r/a$, and where $P_o$ is arbitrary and unitless. For convenience let $P_o = 1$ in the following development.

Shear stress and displacement are related by:

$$\tau_{o\phi z}(r_o,0) = \frac{\partial u_{o1}(r_o,0)}{\partial z_o}$$

Applying the Hankel transform to this equation and to equation (8), the relation between transformed stress and displacement at the surface is:

$$\bar{f}_o(\xi_o) = \frac{\partial \bar{u}_{o1}(r_o,0)}{\partial z_o} \qquad (9)$$

where $\bar{f}_o(\xi_o)$ is the Hankel transform of $f_o(r_o)$. Substituting $\bar{u}_{o1}$ from equation (6) into equation (9) and using equation (7), the coefficients in the first layer are:

$$A_{o1} = \frac{\bar{f}_o(\xi_o)}{\beta_{o1}(\gamma_{o1} - 1)} \tag{10}$$

$$B_{o1} = \frac{\gamma_{o1}\bar{f}_o(\xi_o)}{\beta_{o1}(\gamma_{o1} - 1)} \tag{11}$$

The dimensionless displacement at the surface is obtained by substituting equations (10) and (11) into equation (6), applying the inverse Hankel transform, and setting $z_{o1} = 0$:

$$u_{o1}(r_o,0) = \int_0^\infty \frac{\bar{f}_o(\xi_o)}{\beta_{o1}(\gamma_{o1} - 1)} (\gamma_{o1} + 1)\xi_o J_1(\xi_o r_o) d\xi_o \tag{12}$$

The unscaled displacement is given by:

$$u_1(r,0) = aP_o u_{o1}(r_o,0)$$

To this point the entire derivation has been for an elastic medium. To extend the solution to anelastic media I allow the shear modulus to be a complex valued quantity, the imaginary part of which is a function of frequency (Appendix A).

Stress Boundary Condition

The most straightforward method of determining $\bar{f}_o(\xi_o)$ is to specify the stress beneath the baseplate:

$$\tau_{o\phi z}(r_o,0) = f_o(r_o) \qquad r_o < 1$$

The unknown term $\bar{f}_o(\xi_o)$ is obtained as the Hankel transform of $f_o(r_o)$. I apply two constraints to the choice of the function $f_o(r_o)$: first, $f_o(r_o) = 0$ at $r_o = 0$, and second, I must be able to calculate $\bar{f}_o(\xi_o)$ analytically. The first constraint is required by the physics of the problem. The second constraint makes the problem more manageable numerically.

A general stress distribution which satisfies these requirements is:

$$f_o(r_o) = r_o(1 - r_o^2)^{\nu} \qquad \nu > -1 \qquad (13)$$

and its Hankel transform is:

$$\bar{f}_o(\xi_o) = 2^{\nu}\,\Gamma(\nu + 1)\,\xi_o^{-(\nu+1)}\,J_{\nu+2}(\xi_o) \qquad (14)$$

Since $\nu$ may take on any value greater than -1, a wide variety of stress distributions is possible.

Stress distributions represented by equation (13) are shown in Figure 2. For any value of $\nu$ less than 0 the stress is singular ar $r_o$=1. For $\nu = 0$ the stress varies linearly over the disk from 0 in the center to 1 at the edge. For $\nu > 0$ the stress at $r_o = 1$ is 0.

The stress distribution for $\nu = -1/2$ is that obtained for a statically rotated rigid disk. None of the stresses represented by equation (13) is that of a dynamically rotating rigid disk. These stress distributions represent sources which flex as they

are dynamically rotated. The manner in which they flex is a function of frequency.

Displacement Boundary Condition

If the boundary condition at the source is expressed in terms of the source displacement, the stress that gives rise to this displacement must be calculated to obtain $\bar{f}_o(\xi_o)$. The boundary condition at the surface, written in terms of dimensionless parameters, is:

$$\begin{aligned} u_{o1}(r_o,0) &= P_o g_o(r_o) \qquad r_o < 1 \\ \tau_{o\phi z}(r_o,0) &= 0 \qquad\qquad r_o > 1 \end{aligned} \tag{15}$$

where $g_o(r_o)$ is known and $P_o$ is arbitrary and unitless. For convenience let $P_o = 1$.

Since $u_{o1}$ and $\bar{u}_{o1}$, and $\tau_{o\phi z}$ and $\bar{\tau}_{o\phi z}$ are related by a Hankel transform, equations (15) may be rewritten in the form:

$$\begin{aligned} H_1\{\bar{u}_{o1}(\xi_o,0);r_o\} &= g_o(r_o) \qquad r_o < 1 \\ H_1\left\{\frac{\partial \bar{u}_{o1}(\xi_o,0)}{\partial z_o};r_o\right\} &= 0 \qquad\qquad r_o > 1 \end{aligned} \tag{16}$$

Using equations (6) and (7) these equations become:

$$H_1\{(1+\gamma_{o1})A_{o1}(\xi_o);r_o\} = g_o(r_o) \qquad r_o < 1$$
$$H_1\{\beta_{o1}(1-\gamma_{o1})A_{o1}(\xi_o);r_o\} = 0 \qquad r_o > 1 \tag{17}$$

where the second equation in (17) has been multiplied by -1 for convenience. Equation (17) is a dual integral equation that must be solved for the unknown $A_{o1}(\xi_o)$ to determine the stress beneath the vibrator.

Using a method described in detail by Gladwell (1980) this equation may be reduced to a Fredholm integral equation of the second kind (Dorn, 1980):

$$g_o(x_o) = \psi_o(x_o) + \int_0^1 \psi_o(y_o)M_o(x_o,y_o)dy_o \tag{18}$$

where:

$$M_o(x_o,y_o) = \frac{2}{\pi}\int_0^\infty H_{o1}(\xi_o)\sin(\xi_o y_o)\sin(\xi_o x_o)d\xi_o \tag{19}$$
$$x_o < 1 \qquad r_o < 1$$

$$g_o(x_o) = x_o^{-1}\frac{\partial}{\partial x_o}A_1\{r_o^2 g_o(r_o);x_o\} \qquad r_o < 1 \tag{20}$$

and:

$$H_{o1}(\xi_o) = \left[\frac{(1+\gamma_{o1})}{(1-\gamma_{o1})}\frac{\xi_o}{\beta_{o1}} - 1\right] \tag{21}$$

$A_1$ is the Abel operator defined in Table 1. For $r_o < 1$ and $x_o < 1$, $g_o(x_o)$ is known, $M_o(x_o,y_o)$ may be calculated using equation (19) and equation (18) may be solved for the unknown $\psi_o(x_o)$. The stress beneath the baseplate is given by:

$$\tau_{o\phi z}(r_o,0) = -H_1\ \{F_s\ \{\psi_o(x_o);\xi_o\}\ ;r_o\} \qquad (22)$$

and the Hankel transform of the stress is (Dorn, 1980):

$$\bar{f}_o(\xi_o) = -F_s\ \{\psi_o(x_o);\xi_o\} \qquad (23)$$

for $x_o < 1$ and $r_o < 1$. Once equation (18) is solved for $\psi_o(x_o)$, then $\bar{f}_o(\xi_o)$ may be calculated from equation (23) and the solution for the displacement is obtained from equation (12).

Numerous functions $g_o(r_o)$ could be chosen as the displacement boundary condition. The one condition that all such functions must satisfy for a torsional source is that $g_o(r_o) = 0$ at $r_o = 0$. For ease of calculation I also require that $g_o(x_o)$ be calculated analytically.

Five possible displacement distributions are represented by:

$$g_{o\nu}(r_o) = r_o^{\nu} \qquad \nu = 1,\ldots,5 \qquad (24)$$

The corresponding expressions for $g_o(x_o)$ are:

$$\begin{aligned}
g_{o1}(x_o) &= 2\left(\frac{2}{\pi}\right)^{\frac{1}{2}} x_o \\
g_{o2}(x_o) &= \frac{3}{2}\left(\frac{\pi}{2}\right)^{\frac{1}{2}} x_o^2 \\
g_{o3}(x_o) &= \frac{8}{3}\left(\frac{2}{\pi}\right)^{\frac{1}{2}} x_o^3 \\
g_{o4}(x_o) &= \frac{15}{3}\left(\frac{\pi}{2}\right)^{\frac{1}{2}} x_o^4 \\
g_{o5}(x_o) &= \frac{16}{5}\left(\frac{2}{\pi}\right)^{\frac{1}{2}} x_o^5
\end{aligned} \qquad (25)$$

The displacement distributions represented by equation (24) are shown in Figure 3. For $\nu = 1$ the displacement is that of a perfectly rigid disk. For the remaining values of $\nu$ the outer edge of the disk rotates more than the inner portion. The stress distribution beneath these sources is a function of frequency.

Calculation of the Impedance

As shown in equation (1) the torsional impedance is a function of the total torque and the mean angular displacement given by:

$$\Gamma = -2\pi \int_0^a r^2 f(r)\,dr \tag{26}$$

$$\left(\overline{\frac{u_1}{r}}\right) = \frac{1}{\pi a^2} \int_0^a \int_0^{2\pi} \frac{u_1(r,0)}{r}\, r\,dr\,d\phi \tag{27}$$

Written in terms of dimensionless parameters equations (26) and (27) become:

$$\Gamma_o = -2\pi \int_0^1 r_o^2\, f_o(r_o)\,dr_o \tag{28}$$

$$\left(\overline{\frac{u_{o1}}{r_o}}\right) = 2 \int_0^1 u_{o1}\,dr_o \tag{29}$$

where:

$$\Gamma = \mu_1 a^3 \Gamma_o \tag{30}$$

Using the definitions of $\mu_1$ and $a_o$, equation (1) may be rewritten in terms of dimensionless parameters:

$$Z_T = B_T \rho_1 v_{s1} a^2 \left[ \frac{1}{a_o B_T i} \left( \frac{\Gamma_o}{\pi (\overline{u_{o1}/r_o})} \right) \right] \qquad (31)$$

From equation (31) it is clear that the torsional radiation impedance has units of acoustic impedance ($\rho_1 v_{s1}$) times distance squared ($a^2$). The "extra" factor of $a^2$ occurs because torque per unit area and angular velocity must be used for a torsional source instead of stress and linear velocity, which would be appropriate for a vertical source.

$B_T$ is the zero frequency solution for the quantity in the innermost brackets in equation (31), for an undamped half-space. $B_T$ is factored out because it is a convenient normalization, and most of the dependance of the impedance function on source behavior at low frequencies is contained in $B_T$. For a vertical vibrator $B_V$ is a function of source behavior and Poisson's ratio. For a torsional source $B_T$ is only a function of source behavior.

Equations (28) and (29) show that it is not necessary to set $P_o = 1$ in the stress or displacement boundary conditions. If $P_o$ is not 1, a factor of $P_o$ enters the numerator through the torque term cancelling a factor of $P_o$ that enters the denominator through the displacement term. So as long as the restrictions of elastic theory (infinitesimal stress and strain) are met, the impedance is independent of the amplitude of the

baseplate vibration.

When the surface boundary condition is specified interms of the stress distributions presented in equation (13) the equations for $\Gamma_o$, $(\overline{u_{o1}/r_o})$ and $B_T$ are:

$$\Gamma_o = -\pi \frac{\Gamma(\nu+1)}{\Gamma(\nu+3)} \tag{32}$$

$$\left(\overline{\frac{u_{o1}}{r_o}}\right) = 2 \int_0^\infty \left(\frac{1 + \gamma_{o1}}{1 - \gamma_{o1}}\right) \frac{(J_o(\xi_o)-1)}{\beta_{o1}} \bar{f}_o(\xi_o) d\xi_o \tag{33}$$

$$B_T = \frac{2\Gamma^2(\nu+5/2)}{\Gamma(\nu+3)\{\pi^{\frac{1}{2}}\Gamma(\nu+5/2) - \Gamma(\nu+2)\}} \tag{34}$$

where $\bar{f}_o(\xi_o)$ is given by equation (14).

When the source is defined by using the displacement condition in equation (24) the resulting expressions are:

$$\Gamma_o = 4\sqrt{2\pi} \int_0^1 x_o \psi_o(x_o) dx_o \tag{35}$$

$$\left(\overline{\frac{u_{o1}}{r_o}}\right) = \frac{2}{\nu+1} \qquad \nu = 1,2,\ldots,5 \tag{36}$$

There is no general closed form expression for $B_T$ as a function of $\nu$ for the displacement conditions in equation (24).

Since the quantity in brackets in equation (31) is a complex valued function, the impedance function can always be written in the form:

$$Z_T = B_T \rho_1 v_{s1} a^2 \{R - \frac{i}{a_o} I\} \qquad (37)$$

or:

$$Z_T = B_T \rho_1 v_{s1} a^2 \{A\, e^{i\phi}\}$$

The factor of $a_o^{-1}$ is removed from the imaginary part to eliminate a singularity at $a_o = 0$. R and I are referred to as the equivalent damping and stiffness coefficients, respectively. A and $\phi$ are the dimensionless impedance magnitude and phase. The results presented in this paper will consist of plots of R, I, A and $\phi$ as functions of dimensionless frequency, $a_o$.

Program Tests

Two programs have been written to calculate the radiation impedance of torsional vibrators. TORIMP implements the solution for the stress boundary condition, and TORIES implements the solution for the displacement boundary condition. The accuracy of these programs has been checked by comparing results obtained from them with results in the published literature. In order to compare the program results with the undamped literature solutions, the programs were run with the appropriate source types over a half-space model with a frequency independent $Q = 10^6$, so that the models are essentially undamped.

The accuracy of TORIMP is checked by comparing its results for a stress distribution with $\nu = 0$ with Miller and Pursey's (1954) results, and for $\nu = -1/2$ with Collins' (1962) results. These authors presented results for the radiation impedance at

low dimensionless frequencies. Although Collins' solution is for a dynamically vibrating rigid disk (displacement boundary condition), and the results obtained from TORIMP with $\nu = -1/2$ are for the stress under a ststically rotated rigid disk, at low frequencies good agreement can be anticipated.

The accuracy of TORIES has been checked by comparing its results for a rigid baseplate with those obtained by Collins (1962) and the few tabulated results for the exact solution for a rigid baseplate obtained formally by Sagoci (1944) and tabulated by Stallybrass (1962, 1967).

Table 2 contains the results of these comparisons. The precision of the numbers listed for Miller and Pursey (1954) and Sagoci (1944) is limited by the number of significant figures presented by Miller and Pursey (1954) and Stallybrass (1962, 1967).

## MODEL RESULTS

### Half-Space Models

The equivalent damping and stiffness coefficients (R and I) are shown in Figure 4 as a function of dimensionless frequency for a half-space model. The data shown were calculated for a stress distribution at the source with $\nu = 0$ and a frequency independent $Q = 100$. Several general comments regarding the radiation impedance of a torsional source over a half-space

may be made with reference to this figure. For a massless baseplate over an undamped half-space, R = 0 and I = 1 at $a_o = 0$. The equivalent stiffness (I) is 1 at zero frequency because of the normalization by $B_T$. The dominance of the imaginary part at low frequencies is further accentuated by the fact that $I/a_o$ is singular at $a_o = 0$. As a result, the half-space at low frequencies is purely reactive - it behaves as if the medium consisted of a spring with no dashpot.

At high dimensionless frequencies I remains finite (oscillating in Figure 4) so that $I/a_o$ approaches 0. The real part of the impedance dominates and the half-space is essentially resistive - it reacts as if the medium consisted of a dashpot without any associated spring.

The curves plotted in Figure 4 show oscillations with a period of about $2\pi$. From the definition of dimensionless frequency ($a_o = 2\pi a/\lambda$, where $\lambda$ is the wavelength) it is clear that each increase in $a_o$ by $2\pi$ means that another wavelength of the seismic wave would fit on the baseplate. This combined with the fact that the first oscillation occurs for $a_o > 2\pi$ suggests that the oscillations in the half-space curve may be associated with the number of wavelengths of the seismic wave per baseplate radius.

Kashio (1970) reports similar oscillations in the half-space radiation impedance curves derived for a vertically vibrating foundation. He shows that the resonance is due

to Rayleigh waves originating at one edge of the baseplate interracting with the opposite edge. In the case of the torsional vibrator the effect is caused by the interaction of horizontally travelling SH body waves with the edges of the baseplate. Since the torsional vibrator generates a smaller proportion of waves travelling horizontally as frequency increases (Dorn, 1980) the amplitude of the resonances caused by these waves would be expected to decrease with increasing frequency, as shown in Figure 4.

In Figure 5 the equivalent damping and stiffness coefficients are plotted for 4 different sources over a half-space model. The sources used were a rigid baseplate (displacement boundary condition, $\nu = 1$), and three flexible baseplates (stress boundary condition, $\nu = -1/2$, 0 and 1). For $a_o$ less than 1 the equivalent stiffness and damping are relatively independent of source type. The effect of changing source type at low frequencies has been absorbed into the term $B_T$. As shown in Tables 2 and 3 $B_T$, and as a result the impedance $Z_T$, decreases as $\nu$ increases for the stress distributions and as $\nu$ decreases for the displacement distributions. Qualitatively this means that the low frequency radiation impedance decreases as the outer portion of the disk rotates through a smaller angle than the inner portion of the source.

The oscillations described earlier are present for all source types excepth the rigid baseplate. Although the oscillation period remains nearly constant at $2\pi$, the location of the

first peak or trough and the oscillation amplitude depends on the source type.

The effects of anelasticity on the radiation impedance are shown in Figure 6. The model consists of a torsional source defined by a stress distribution with $\nu = 0$, on the surface of a homogeneous, isotropic half-space. The quality factor (Q) is independent of frequency and ranges in value from 100 to 2.

The presence of frequency independent damping in the model produces a singularity in the equivalent damping coefficient at $a_o = 0$ because the imaginary part of the complex shear modulus for this type of damping does not approach 0 as $a_o$ goes to 0. The width of the singularity increases as damping increases (Q decreases). The oscillations in the real part of the impedance function are rapidly damped out, but are apparent in the imaginary part of the impedance even for Q = 2. As damping increases the imaginary part becomes increasingly negative in value. Although the magnitude of the oscillations is a function of the damping, the location of the peaks and troughs in the stiffness and damping coefficients is independent of damping.

The real and imaginary parts of the radiation impedance (R and I) are unitless functions of dimensionless frequency. For a half-space model, R and I are completely independent of the density and shear wave velocity. This result is shown in Figure 7. The top pair of plots present the results obtained for the equivalent damping and stiffness coefficients

for three different models. These models have densities of 2, 2 and 4 g/cm$^3$ and velocities of 2.5, 5 and 2.5 km/sec respectively. In each case the source is represented by a stress distribution with $\nu = 0$. The medium has a Q of 100.

All three models produce exactly the same curves for the equivalent stiffness and damping. For a half-space model, all of the dependance on density and velocity is contained in the product $\rho v_s$ in equation (37).

If the total torque and mean angular velocity are measured in the field and $Z_T$ is calculated, then:

$$Z_T = R_z - \frac{i}{f} I_z \tag{38}$$

where f is the frequency in Hertz and where:

$$R_z = \text{Real } (Z_T) = B_T \rho v_s a^2 R \tag{39}$$

$$I_z = \left(\frac{-f}{i}\right) \text{Imag.}(Z_T) = \frac{B_T \rho v_s^2}{2\pi} I \tag{40}$$

The functions $R_z$ and $I_z$ defined by equations (39) and (40) are plotted for the three half-space models as a function of frequency (f) in kHz in the lower pair of plots in Figure 7. Although the dimensionless parameters R and I are unnaffected by changes in density and velocity for a half-space, the real and imaginary parts of $Z_T$ are affected. As velocity decreases both the amplitude and frequency of the oscillations decrease. As density decreases only the amplitude of the

oscillation decreases, the frequency does not change. The amplitude effects are caused by the $\rho v_s$ product in equation (37). The frequency shift is inherent in the relationship between dimensionless frequency ($a_o$) and frequency (f).

The locations of the oscillations in R and I for a half-space are independent of velocity, density and damping, and are only a function of the source type. Suppose that the behavior of a torsional source is known in terms of its stress or displacement distribution. Then regardless of the half-space on which it vibrates, the first peak in the equivalent damping coefficient will always occur at the same dimensionless frequency, $a_1$. If the actual frequency of this first peak, $f_1$, could be measured, then the definition of dimensionless frequency provides a relation to determine the shear wave velocity of the half-space:

$$v_s = \frac{2\pi f_1 a}{a_1} \qquad (41)$$

Suppose for the particular source being used that the first peak in the equivalent damping occurs at a dimensionless frequency $a_1 = 2\pi$, the baseplate radius is 0.5 meters, and the shear velocity of the medium is 500 m/sec. Then, solving equation (41) for the frequency $f_1$, the first peak would occur at a freauency of 1000 Hz. This is well beyond the range of hydraulically actuated exploration vibrators. If the baseplate

radius is doubled, the frequency of the first resonance is reduced to 500 Hz. Such frequencies might be obtained by an electromagnetically actuated vibrator.

All impedance results discussed to this point assume a massless baseplate. A method of including the baseplate mass in the radiation impedance for a torsional vibrator has been described by Robertson (1967). The equation for the impedance, including the baseplate mass, is:

$$Z_T = B_T \rho v_s a^2 \left( R - \frac{i}{a_o} I' \right) \tag{42}$$

where:

$$I' = I - \frac{3}{16} M_o a_o^2 \tag{43}$$

and:

$$M_o = M/(\rho a^5) \tag{44}$$

where M is the moment of inertia of the baseplate.

From equations (42) and (43), the imaginary part of the impedance function is:

$$\frac{I'}{a_o} = \frac{I}{a_o} - \frac{3}{16} M_o a_o \tag{45}$$

Although $I/a_o$ approaches 0 as $a_o$ becomes large, the second term in equation (45) becomes infinite as $a_o$ approaches infinity. A plot of I' as a function of $a_o$ (Figure 8) shows that the equivalent stiffness coefficient rapidly acquires

large negative values as $a_o$ increases.

The magnitude and phase of the impedance are also shown in Figure 8. The baseplate mass produces a minimum in the impedance magnitude, the frequency of which depends on the baseplate mass. Robertson (1967) has suggested that this phenomenon could be used to determine the shear modulus of the medium. Using a similar method, the shear velocity of the medium can be calculated. From equations (42) and (43) a plot can be constructed of the frequency ($a_{omin}$) at which the minimum in impedance magnitude occurs as a function of the dimensionless moment of inertial $M_o$. If the density of the medium can be estimated or determined in some fashion, then the baseplate mass can be adjusted to achieve any desired dimensionless moment of inertia. The frequency of vibration of the baseplate could be varied until the freauency of the minimum impedance is attained ($\omega_{min}$). The shear velocity is then computed from the equation:

$$v_{s1} = \frac{\omega_{min} a}{a_{omin}} \qquad (46)$$

The advantage of determining the shear wave velocity of the medium using the method based on the location of the half-space oscillation peak is that the shear velocity is determined independently of any other physical parameters. The method described here relies on an independent determination of the density of the medium. The first method has the disadvantage of requiring either very large baseplates (a > 1 m)

or very high frequencies ($a_o$ > 500 Hz), while the method that relies on the baseplate mass could be arranged to yield results at much lower frequencies.

Layered Models

Typical results obtained for a model involving a single layer over a half-space are shown in Figure 9 as the solid curves. The scaled thickness of the layer was 3.0 and the shear wave velocities of the layer and the half-space were 2 and 2.5 km/sec, respectively. The densities of the layer and the half-space were 1.5 and 2 g/cm$^3$ and Q was 100. The source was defined by a stress distribution with $\nu = 0$. The dashed curve of Figure 9 was obtained for a half-space model.

A layered model produces an impedance curve that oscillates about the curve due to a half-space. The amplitude of the oscillations due to the layer (the layer resonance) increases as a function of frequency for low levels of damping.

The effects of changing thickness of the surface layer on the impedance function are shown in Figure 10. Equivalent damping coefficients are plotted for four different layer thicknesses ranging from a scaled thickness ($h_{o1} = h_1/a$) of 0.5 to 3.0. In each case the velocities of the surface layer and the half-space are 2.0 and 2.5 km/sec, and the densities are 1.5 and 2.0 g/cm$^3$, respectively. A frequency independent Q = 100 is used in both the layer and the half-space. The source is defined by a stress distribution with $\nu = 0$. Only

the equivalent damping coefficients are presented since the equivalent stiffness coefficients show similar features.

As the thickness of the surface layer increases, both the period ($P_o$ in Figure 11) and the amplitude of the layer resonance decrease. In the limit as the scaled thickness approaches 0 or $\infty$ a half-space impedance curve results.

The physical process that gives rise to these results is revealed by a study of the layer resonance. With the half-space trend removed, the resonance due to the layer oscillates around 0 and, for thick layers (eg a scaled thickness of 3 or more), this oscillation appears to be very nearly sinusoidal. Subtracting the half-space impedance from the results for a layer with a scaled thickness of 5, and using an FFT to obtain a time domain representation of the residual layer resonance, results in the plot shown in Figure 11.

The two way travel time for a seismic wave to travel vertically from the surface to the layer interface and back is:

$$T = \frac{2h_1}{v_{s1}} \tag{47}$$

If an impulse is measured at time T on the surface, the Fourier transform of the impulse would be a sine wave with a period given by:

$$P = 1/T \tag{48}$$

Using the definition of dimensionless frequency, $P_o$ (dimensionless period) and P are related by:

$$P = \frac{v_{s1}}{2\pi a} P_o \tag{49}$$

Using equations (47), (48) and (49) there are simple relations between the scaled thickness of the surface layer , the dimensionless period of the layer resonance, and the dimensionless arrival time of the impulse:

$$P_o = \frac{\pi}{h_{o1}} \tag{50}$$

$$T_o = \frac{h_{o1}}{\pi} \tag{51}$$

Substituting the thickness of the layer used to generate Figure 11 into equation (51), the dimensionless two way travel time is 1.59. This is exactly the arrival time shown for the first event in Figure 11. It also is the separation between each successive event. The layer resonance, then, is primarily due to seismic waves being reflected between the baseplate and the layer interface. Figure 11 shown the first arrival as well as the first, second and third multiples. The amplitude fall-off between multiples is due to a combination of material damping, spreading of of the wavefront from the finite-sized source, and the reflection coefficient of the layer/half-space interface.

Equation (50) may be successfully applied to layered impedance curves in the literature for vertical and horizontal vibrators to determine either the period from a given thickness or the thickness from measured period. This suggests that the layer resonance for those vibrators is also primarily due to reflections.

The layer resonance amplitude decreases to nearly 0 as dimensonless frequency approaches 0 because at low frequencies the torsional vibrator is a poor radiator in near vertical directions. Since vertical and horizontal vibrators radiate relatively efficiently vertically at low frequencies (Miller and Pursey, 1954; Cherry, 1962), the layer resonance would be expected to continue with a large amplitude at low frequencies. The conclusion is supported by the results of Luco (1974).

An intriguing possibility exists in determining the unnormalized layer thickness from the impedance function. If the shear velocity of the first layer can be obtained using one of the methods described earlier, then the thickness of the layer could be obtained from the dimensionless period of the layer resonance:

$$h_1 = \frac{a\pi}{P_o} \tag{52}$$

Since the layer resonance is primarily due to reflections, the acoustic impedance contrast across the interface ($\rho_1 v_{s1}/\rho_2 v_{s2}$) should play an important role in the response. Figures 12 and 13 present the equivalent damping coefficients

obtained for several models with varying velocity and density contrasts. The base model in each case is a single layer with a scaled thickness of 1 over a half-space. The density and velocity of the lower half-space are 2 g/cm$^3$ and 2.5 km/sec, respectively, and remain constant for all models. In Figure 12 the density of the surface layer is varied while the shear velocity of the layer is a constant 2.5 km/sec. In Figure 13 the velocity of the surface layer varies while the density is a constant 2 g/cm$^3$. In each figure, the solid curves were obtained for models with $\rho_1 v_{s1} > \rho_2 v_{s2}$, while the dashed curves represent models with $\rho_1 v_{s1} < \rho_2 v_{s2}$.

In Figure 12 the density of the surface layer is 6, 4, 1 and 0.667 g/cm$^3$. These values were chosen so that the ratio of acoustic impedances of the layer over the half-space has values of 3, 2, 1/2 and 1/3. These same values of acoustic impedance contrast are used in Figure 13 by choosing velocities in the first layer to be 7.5, 5, 1.25 and 0.8333 km/sec. So in each of the two figures, the acoustic impedance contrasts represented by the solid and dashed curves is the same in magnitude but opposite in sense. Also, the acoustic impedance contrasts for curves in Figure 12 are the same as the acoustic impedance contrasts for the corresponding curves in Figure 13.

From Figures 12 and 13 it is apparent that a change in the sense of the acoustic impedance contrast causes a 180$^o$ phase shift in the layer resonance. The solid curves have peaks where the dashed curves have troughs. This result could

have been readily predicted. Since most of the response is due to reflections of nearly vertically travelling waves by the layer interface, plane wave theory predicts a change in the sign of the reflection coefficient depending on the sense of the acoustic impedance contrast.

As expected, the resonance amplitude increases as the contrast in acoustic impedance increases because a greater proportion of the seismic energy incident upon the interface is reflected.

A comparison of the solid curves in Figures 12 and 13 shows that, for a given acoustic impedance contrast, the curves are essentially identical regardless of whether the contrast is due to a high density or a high velocity in the surface layer. However, a comparison of the dashed curves in these two figures reveals that the curves for a low density surface layer are noticeably different from the curves for a low velocity surface layer. The most significant differences are the amplitude of the resonances, especially the resonance peak located near $a_o = 10$, and the shift in locations of the peaks for the low velocity surface layers.

A possible explanation for the differences associated with a low velocity surface layer is suggested by studying a hypothetical model in which the layer and the underlying half-space have the same acoustic impedance, but have different velocities and densities. The results for a series of models with no acoustic impedance contrast, but with density and

velocity contrasts, are shown in Figure 14. The solid curve was obtained for a half-space with a source having a stress distribution with $\nu = 0$, and a frequency independent $Q = 100$.

Two curves are plotted in addition to the half-space impedance function, although one of these curves is only evident on the plot of the equivalent stiffness coefficient. For the dashed curves the densities for the layer and the underlying half-space are 4 and 2 $g/cm^3$, respectively, and the respective velocities are 2 and 4 km/sec. These layered models have a low velocity surface layer over a high velocity half-space. For the curve plotted with the long dashes, the scaled layer thickness is 0.5. For the curve with short dashes, the scaled thickness of the overburden is 3. For the thin layer, the presence of the low velocity layer results in an impedance function that shows resonances similar to those caused by reflections. As the thickness increases these resonances rapidly disappear. Since there is no acoustic impedance contrast, and since the "resonance" effect occurs only for very thin layers with a low velocity overlying a high velocity half-space, these resonances are apparently due to refracted arrivals.

Using ray theory, and the velocity contrast used in Figure 14, if the layer has a scaled thickness less than 1.732 it is possible for energy from one edge of the baseplate to be refracted and to interract with the opposite edge. Modelling shows that as the scaled thickness exceeds 1.732 for this

velocity contrast, the resonance rapidly disappears and the response returns to the half-space impedance curve.

The results obtained for a layered model with varying hysteretic damping are shown in Figure 15. The model consists of a single layer of scaled thickness 1 over a half-space. The shear velocity and density are 2 km/sec and 1.5 $g/cm^3$ for the surface layer and 2.5 km/sec and 2 $g/cm^3$ for the half-space. A stress distribution with $\nu = 0$ is used at the source and the quality factor (Q) has values of 100, 10, 3.3 and 2. These values are the same as those used for the half-space models shown in Figure 6 so that a direct comparison may be made.

Comparing Figures 15 and 6, the effect of the layer on the impedance function is evident at all damping levels except Q = 2. As the damping increases, the amplitude of the layer resonance decreases, and the curves become more similar to those obtained for a half-space.

One problem of particular interest to exploration seismologists is the determination of weathered layer parameters including the thickness and seismic velocity. In order to assess the feasability of using radiation impedance measurements to determine the thickness of the weathered layer, impedance functions are presented in Figure 16 for several models that incorporate values of density, velocity and damping that might be encountered in a field survey.

The model used in Figure 16 is a single layer over a half-space with both media having a frequency independent Q of 10. The velocity and density are 0.3 km/sec and 1.3 g/cm$^3$ in the surface layer, and 2.4 km/sec and 2.6 g/cm$^3$ for the lower half-space. Curves are presented for three different scaled thicknesses of the weathered layer.

As shown in the graph, the layer resonance is detectable for layers that are 1 or 3 baseplate radii thick. However, the impedance for a layer 5 baseplate radii thick is indistinguishable from the half-space impedance function. This result is significant because most weathered material with the shear velocity and density used in these models would have a quality factor on the order of 10. So for typical surface materials, the torsional impedance would not show any effect due to the interface between the weathered layer and the material below it unless the layer thickness is less than about 5 baseplate radii.

The radiation impedance for a two layered model is shown in Figure 17 along with the curve for the same surface layer but with the second interface removed. The shear wave velocities, starting with the surface layer, are 1, 2 and 3 km/sec, and the densities are 1.5, 1.5 and 2 g/cm$^3$. The frequency independent quality factor is 100 for all layers. The surface layer has a scaled thickness of 1 and the second layer is 0.5 baseplate radii thick.

The difference between the two layer impedance function

(solid curves) and the one layer impedance funciton (dashed curves) is clear. The dominant oscillation in the two layer curves is due to the surface layer. There are secondary oscillations and distortions introduced by the second interface. The dominant period of the resonance could be estimated fairly reliably from these results. However, it is unlikely that the secondary period related to the depth to the second interface, or any other period due to various multiples, could be determined reliably from such data.

## CONCLUSIONS

In this paper the problem of vibrator - earth interaction has been studied by calculating the radiation impedance of torsionally vibrating sources on the surface of a plane-layered anelastic medium.

The torsional radiation impedance for a half-space is a function of source behavior, material properties and baseplate mass. The oscillations in the impedance for a flexible baseplate on a half-space are caused by horizontally travelling SH body waves interacting with the baseplate. The spacing between peaks or troughs is related to the number of wavelengths per baseplate radius. The exact dimensionless frequency at which the peaks and troughs occur is a function of source behavior, but is not a function of material properties. If the baseplate

behavior is known, a measurement of the frequency (Hz) at which the first resonance occurs would provide a means of estimating the shear wave velocity of the medium. The primary difficulty with this procedure is that for shear wave velocities encountered in the weathered layer the source must either operate at frequencies between 500 and 1000 Hz, or the baseplate radius must be somewhat larger than 1/2 meter. An electromagnetically actuated vibrator might operate in the necessary frequency range.

At low frequencies, the effect of changing source behavior is contained in the term $B_T$, the static solution of the equivalent stiffness coefficient. As the source becomes more flexible $B_T$ decreases so that the total torque required to impart a given signal to the medium decreases. This suggests that a vibrator's efficiency might be increased by modifying the structure or strength of the baseplate.

Increasing the amount of anelasticity in the medium decreases the amplitude of the half-space resonance. However, if the quality factor is independent of frequency, the oscillations are still noticeable for Q as low as 3.

The baseplate mass modifies the imaginary part of the impedance function and produces a minimum in the impedance magnitude. The dimensionless frequency at which this minimum occurs is a function of the dimensionless moment of inertia of the baseplate. This effect could be used to estimate the

shear wave velocity of the medium if an estimate of the density is made independently.

The presence of a layer results in an impedance function that oscillates around the impedance due to a half-space. the period of the oscillation and the amplitude both vary inversely with the thickness of the layer. This layer oscillation is a resonance effect produced by near vertical reflections between the layer interface and the baseplate. If the shear wave velocity of the medium is known, the period of the resonance may be used to provide a reliable estimate of the layer thickness.

The layer resonance amplitude decreases as frequency approaches 0 because the preferred direction of radiation from a torsional source at low frequencies is horizontal. As shown by Miller and Pursey (1954) and Cherry (1962) horizontal and vertical vibrators produce large displacements in the vertical direction even at low frequencies. As a result, the layer resonance produced by those sources should persist as frequency approaches 0. The modelling results obtained by Kashio (1970) and Luco (1974, 1976) support this conclusion.

The amplitude of the layer resonance increases as acoustic impedance contrast increases, but the location of the resonance peaks and troughs is independent of the contrast. When the sense of the contrast is changed from a lower to a higher velocity in the surface layer, the layer resonance undergoes

a $180^{o}$ phase shift, as the plane wave reflection coefficient would suggest.

The amplitude of the layer resonance also decreases as damping increases. The combined effects on the amplitude of the layer resonance due to material damping and thickness indicate that impedance measurements made over a weathered layer with a Q of 10 and a thickness greater than about 5 baseplate radii will show only a half-space response. As a result, it would be very unlikely that the presence of a second interface at depth would be detected using the radiation impedance.

It would be useful to study the impedance function in more detail in the frequency range in which exploration vibrators operate ($a_o < 1$). The primary interest might be more directed toward the idea of matching the baseplate to the particular medium on which it is to vibrate. A possible method of overcoming the problem of a relatively small baseplate, and as a result a low dimensionless frequency, might be to operate several sources close to each other. Radiation pattern modelling (Dorn, 1980) suggests that there would be little effect due to mutual coupling if the sources are placed about 5 baseplate radii apart.

If design problems could be overcome in building a vibrator with a sufficiently high frequency range and a large enough baseplate to make use of the procedures discussed here to obtain material properties, there are still several practical

problems to overcome in actually measuring the radiation impedance. For a torsional source, the impedance is defined as the total torque divided by the mean angular velocity. Although the total torque might be readily measured in an actual experiment, it probably would not be possible to obtain the mean velocity as defined in this thesis. It would be possible, however, to measure the velocity at a point near the baseplate - either laterally or vertically displaced slightly. The effect of this approximation on the impedance function should be determined.

ACKNOWLEDGEMENTS

I would like to acknowledge the valuable advice and suggestions of Dr. W. E. Farrell of Systems, Science and Software, and Professors H. F. Morrison and L. Johnson of the University of California, Berkeley, all of whom helped guide this research. This study was supported in part by the Department of Energy through Lawrence Berkeley Laboratory under contract number GF 26760, and in part by the Director, Office of Basic Energy Sciences, Division of Engineering, Mathematics and Geosciences of the U.S. Department of Energy under contract No. W-7405-ENG-48.

# APPENDIX A

For a problem that involves only shear waves material damping may be included in the model by allowing the shear modulus to be a complex quantity:

$$\mu^*(\omega) = \mu_R(\omega) + i\mu_I(\omega)$$

with real and imaginary parts which are functions of frequency. This may be written in the form:

$$\mu^*(\omega) = \mu_R(\omega)\ (1 + i\theta(\omega))$$

The use of such a shear modulus has been discussed in detail by Futterman (1962) and Konamori and Anderson (1977).

For the purposes of this paper, the simplification is made of assuming a $\mu_R$ independent of frequency, such that in the mth layer:

$$\mu_m^* = \mu_m(1 + i\theta_m)$$

where $\mu_m$ is the real shear modulus and $\theta_m$ is the specific dissipation constant. The specific dissipation constant and the quality factor are inversely related:

$$Q_m = 1/\theta_m$$

and:

$$\theta_m = \Psi_m \{a_o v_{s1}/v_{sm}\}^j$$

where $\Psi_m$ is called the damping constant and is independent of frequency, and where j is arbitrary. Thus if j = 0 $Q_m$ is independent of frequency and the medium is hysteretically damped. If j = 1, $Q_m$ is inversely proportional to frequency and the medium has Voigt damping.

Table 1

List of Symbols

$a$ = Baseplate radius

$a_o$ = $\omega a/v_{s1}$, dimensionless frequency

$A$ = Magnitude of torsional radiation impedance

$A_m$ = Coefficient for displacement of downgoing wave in mth layer

$B_m$ = Coefficient for displacement of upgoing wave in mth layer

$B_T$ = Zero frequency limit for impedance function

$f$ = frequency

$f(r)$ = Stress under baseplate

$\bar{f}(\xi)$ = $J_1$ Hankel transform of $f(r)$

$g(r)$ = Displacement under baseplate

$g(x)$ = Abel transform of $g(r)$

$h_m$ = Thickness of mth layer

$i$ = $\sqrt{-1}$

$I$ = Equivalent stiffness coefficient

$J_1$ = First order Bessel function of the first kind

$k_s$ = Shear wave number

$P_o$ = Dimensionless magnitude in stress or displacement boundary condition

$Q$ = Quality factor

$r$ = Radial distance from center of baseplate

$R$ = Equivalent damping coefficient

$t$ = Time

$u$ = Displacement

$v_s$ = Shear wave velocity

$z_m$ = Depth below the top of the mth layer, positive down

$Z_T$ = Torsional radiation impedance

Table 1

List of Symbols (cont.)

$\beta_m = (\xi^2 - k_{sm}^2)^{\frac{1}{2}}$

$\gamma_m = B_m/A_m$

$\Gamma$ = Total torque

$\Gamma(\nu)$ = Gamma function

$\lambda$ = Lame's constant

$\mu$ = Shear modulus

$\omega$ = Angular frequency

$\phi$ = Azimuthal angle

$\psi(x)$ = Unknown in Fredholm integral equation of the second kind

$\Psi$ = Damping constant

$\rho$ = Density

$\tau_{\phi z}$ = Stress, subscripts indicate component of stress tensor in cylindrical coordinates

$\theta$ = Phase of torsional radiation impedance

$\Theta$ = Specific dissipation constant

$\xi$ = Hankel transform variable

$\nabla$ = Gradient operator

$\nabla^2$ = Laplacian operator

Subscripts: m = mth layer

s = Shear wave

o = Parameter is dimensionless; parameters with units of distance are normalized by baseplate radius, a; parameters with units of stress are normalized by shear modulus, $\mu_1$.

Mathematical Transforms:

$$\text{Hankel:} \quad H_j\{E(r,z);\xi\} = \int_0^\infty E(r,z) r J_j(\xi r)\, dr$$

$$\text{Fourier Sine:} \quad F_s\{f(t);x\} = \sqrt{2/\pi} \int_0^\infty f(t)\sin(xt)\, dt$$

Table 1

List of Symbols (cont.)

Abel:

$$A_1\{f(t);x\} = \sqrt{2/\pi} \int_0^x \frac{f(t)\,dt}{\sqrt{x^2-t^2}}$$

$$A_2\{f(t);x\} = \sqrt{2/\pi} \int_x^\infty \frac{f(t)\,dt}{\sqrt{t^2-x^2}}$$

Table 2

Comparison of Numerical Results with Literature Solutions

| $a_o$ | Miller & Pursey (1954) | TORIMP $r_o$ | Collins (1962) | TORIMP $r_o(1-r_o^2)$ | Sagoci (1944) | TORIES $r_o$ |
|---|---|---|---|---|---|---|
| **Equivalent Damping Coefficient** | | | | | | |
| 0.1 | .0011 | .00109 | .00141 | .00142 | | .00141 |
| 0.2 | .0043 | .00427 | .00553 | .00554 | .0055 | .00554 |
| 0.3 | .00936 | .00937 | .01209 | .01212 | | .01212 |
| 0.4 | .0161 | .01614 | .02061 | .02075 | | .02078 |
| 0.5 | .0243 | .02426 | .03042 | .03098 | .0310 | .03104 |
| 0.6 | | | | | | .04243 |
| 0.7 | | | | | | .05450 |
| 0.8 | | | | | .06680 | .06685 |
| 0.9 | | | | | | .07919 |
| 1.0 | | | | | .09129 | .09127 |
| 2.0 | | | | | .18313 | .18310 |
| 3.0 | | | | | .23592 | .23591 |
| 4.0 | | | | | .26675 | .26674 |
| 5.0 | | | | | .27819 | .27816 |
| **Equivalent Stiffness Coefficient** | | | | | | |
| 0.1 | 1.00 | .99820 | .99801 | .99782 | | .99801 |
| 0.2 | .99 | .99291 | .99217 | .99142 | .99 | .99216 |
| 0.3 | .984 | .98436 | .98285 | .98113 | | .98280 |
| 0.4 | .973 | .97294 | .97068 | .96748 | | .97045 |
| 0.5 | .959 | .95910 | .95655 | .95110 | .956 | .95572 |
| 0.6 | | | | | | .93924 |
| 0.7 | | | | | | .92162 |
| 0.8 | | | | | .9034 | .90337 |
| 0.9 | | | | | | .88491 |
| 1.0 | | | | | .8666 | .86658 |
| 2.0 | | | | | .71350 | .71350 |
| 3.0 | | | | | .61930 | .61934 |
| 4.0 | | | | | .59068 | .59090 |
| 5.0 | | | | | .60205 | .60272 |

Table 3

$B_T$ for Stresses of the Form $r_o(1 - r_o^2)^\nu$

| $\nu$ | Exact | Approx. |
|---|---|---|
| -0.5 | $\frac{16}{3\pi}$ | 1.6977 |
| 0.0 | $\frac{9\pi}{4(3\pi-4)}$ | 1.3030 |
| 1.0 | $\frac{75\pi}{8(15\pi-16)}$ | .9463 |
| 2.0 | $\frac{1225\pi}{64(35\pi-32)}$ | .7714 |
| 3.0 | $\frac{19845\pi}{128(315\pi-256)}$ | .6639 |

Table 4

$B_T$ for Displacements of the Form $r_o^\nu$

| $\nu$ | Exact | Approx. |
|---|---|---|
| 1.0 | $\frac{16}{3\pi}$ | 1.6977 |
| 2.0 | $\frac{9}{4}$ | 2.2500 |
| 3.0 | $\frac{128}{15\pi}$ | 2.7162 |
| 4.0 | $\frac{25}{8}$ | 3.1250 |
| 5.0 | $\frac{1152}{105\pi}$ | 3.4923 |

# REFERENCES

Arnold, R. N., G. N. Bycroft and G. B. Warburton, 1955, Forced vibrations of a body on an infinite elastic solid: J. of Appl. Mech., v. 22, p. 391 - 400.

Awojobi, A. O. and P. Grootenhuis, 1965, Vibration of rigid bodies on semi-infinite elastic media: Proc. of Roy. Soc. A, v. 287, p. 27 - 63.

Bycroft, G. N., 1956, Forced vibrations of a rigid circular plate on a semi-infinite elastic space and an elastic stratum: Philos. Trans. Roy. Soc. of Lon. A, v. 248, p. 327 - 368.

Collins, W. D., 1962, The forced torsional oscillations of an elastic half-space and an elastic stratum: Proc. London Math. Soc., v. 3, p. 226 - 244.

Dorn, G. A., 1980, Radiation impedance and radiation patterns of torsionally vibrating seismic sources: Ph.D. thesis, Univ. of California, Berkeley.

Futterman, W. I., 1962, Dispersive body waves: J. Geophys. Res., v. 67 No. 13, p. 5279 - 5291.

Gladwell, G. M. L., 1980, Contact problems in the classical theory of elasticity: Sijthoff and Noordhoff.

Kanamori, H., and D. L. Anderson, 1977, Importance of physical dispersion in surface wave free oscillation problems - review: Rev. of Geoph. amd Space Phys., v. 15 No. 1, p. 105 - 112.

Kashio, J., 1970, Steady state response of a circular disk resting on a layered medium: Ph.D. thesis, Rice Univ.

Luco, J. E., 1974, Impedance functions for a rigid foundation on a layered medium: Nuc. Eng. and Design, v. 31, p. 204 - 217.

Luco, J. E., 1976, Vibrations of a rigid disc on a layered viscoelastic medium: Nuc. Eng. and Design, v. 36, p. 325 - 340.

Miller, G. F., and H. Pursey, 1954, The field and radiation impedance of mechanical radiators on the free surface of a semi-infinite isotropic solid: Proc. Roy. Soc. Lond. Ser. A, v. 223, p. 521 - 541.

Robertson, I. A., 1967, On a proposed determination of the shear modulus of an isotropic elastic half-space by forced torsional oscillations of a circular disk: Appl. Sci. Res., v. 17, p. 305 - 312.

Sagoci, H. F., 1944, Forced torsional oscillations of an elastic half-space II: J. of Appl. Phys., v. 15, p. 655 - 662.

Stallybrass, M. P., 1962, A variational approach to a class of mixed boundary value problems in the forced oscillations of an elastic medium: Proc. 4th U. S. Natl. Cong. of Appl. Mech., v. 1, p. 391 - 400.

Stallybrass, M. P., 1967, On the Reissner - Sagoci problem at high frequencies: Int. J. of Engng. Sci., v. 5, p. 689 - 703.

Thomas, D. P., 1968, Torsional oscillations of an elastic half-space: Quart. J. of Mech. and Appl. Math., v. 21, p. 51 - 65.

Wei, Y. T., 1971, Steady state response of certain foundation systems: Ph.D. thesis, Rice Univ.

FIGURE CAPTIONS

Figure 1: The N-layered elastic medium with a cylindrical coordinate system centered at the source. The Nth layer is the lower half-space, $h_{om}$ and $z_{om}$ are the scaled (dimensionless) thickness and depth of the mth layer, and $u_{om}$ is the dimensionless displacement in the mth layer. [XBL 814-2897]

Figure 2: The scaled stress $f_o(r_o)$, beneath the baseplate. [XBL 814-2898]

Figure 3: The scaled displacement, $g_o(r_o)$, of the baseplate. [XBL 814-2899]

Figure 4: The equivalent damping (R) and equivalent stiffness (I) coefficients for a torsional source over a half-space. The source is represented by a stress distribution with $\nu = 0$. [XBL 814-2900]

Figure 5: The effect of varying source type on the radiation impedance for a half-space. Represented are a rigid source (solid curve, displacement boundary condition) and three flexible sources (dashed curves, stress boundary condition). [XBL 814-2901]

Figure 6: The effect of hysteretic damping on the radiation impedance for a half-space. [XBL 814-2902]

Figure 7: The effect of changing velocity and damping on the radiation impedance for a half-space. The equivalent damping and stiffness (top pair of plots) are identical for all three models. The real and imaginary parts of $Z_T$ for the three models are shown in the bottom pair of plots. [XBL 814-2903]

Figure 8: The effect of baseplate mass on the radiation impedance for a rigid source over a half-space [XBL 814-2904]

Figure 9: An example of the torsional radiation impedance for a single layer over a half-space. The layer has a dimensionless thickness of 3, and the half-space curve (dashed curve) is presented for comparison. [XBL 814-2905]

Figure 10: The effect of changing thickness of the surface layer on the radiation impedance. [XBL 814-2906]

FIGURE CAPTIONS (continued)

Figure 11: The Fourier transform of the layer resonance. [XBL 814-2907]

Figure 12: The effect of changing density contrast on the equivalent damping coefficient, plotted for various values of the ratio $\rho_1 v_{s1}/\rho_2 v_{s2}$. [XBL 814-2908]

Figure 13: The effect of changing velocity contrast on the equivalent damping coefficient, plotted for various values of the ratio $\rho_1 v_{s1}/\rho_2 v_{s2}$. [XBL 814-2909]

Figure 14: The effect of a velocity contrast when there is no acoustic impedance contrast. The surface layer has a lower velocity than the half-space. [XBL 814-2910]

Figure 15: The effect of hysteretic damping on the radiation impedance for a single layer over a half-space. [XBL 814-2911]

Figure 16: The detectability of the layer/half-space interface for a "typical" weathered layer. The velocity and density are 0.3 km/sec and 1.3 g/cm$^3$ for the layer and 2.4 km/sec and 2.6 g/cm$^3$ for the half-space. The frequency independent Q is 10. [XBL 814-2912]

Figure 17: The radiation impedance for a model with two layers over a half-space. The solid curves represent the two layered model; the dashed curves represent the same model with the depth to the second interface extended to infinity (effectively a one layer over a half-space model). [XBL 814-2913]

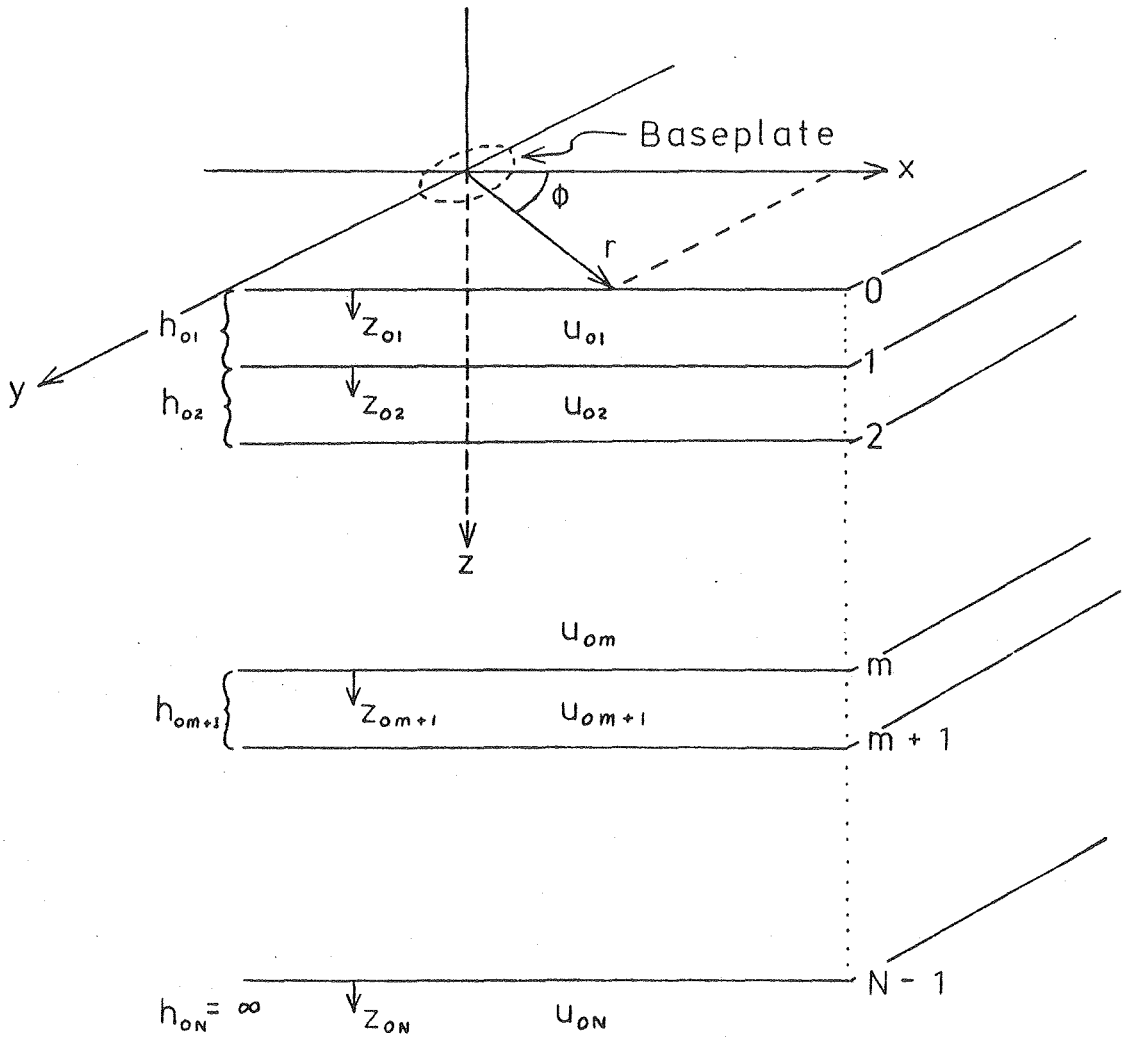
Baseplate
x
ϕ
r
y
z
$h_{o1}$
$z_{o1}$
$u_{o1}$
0
1
$h_{o2}$
$z_{o2}$
$u_{o2}$
2
$u_{om}$
m
$h_{om+1}$
$z_{om+1}$
$u_{om+1}$
m + 1
N - 1
$h_{oN} = \infty$
$z_{oN}$
$u_{oN}$

XBL 814-2897

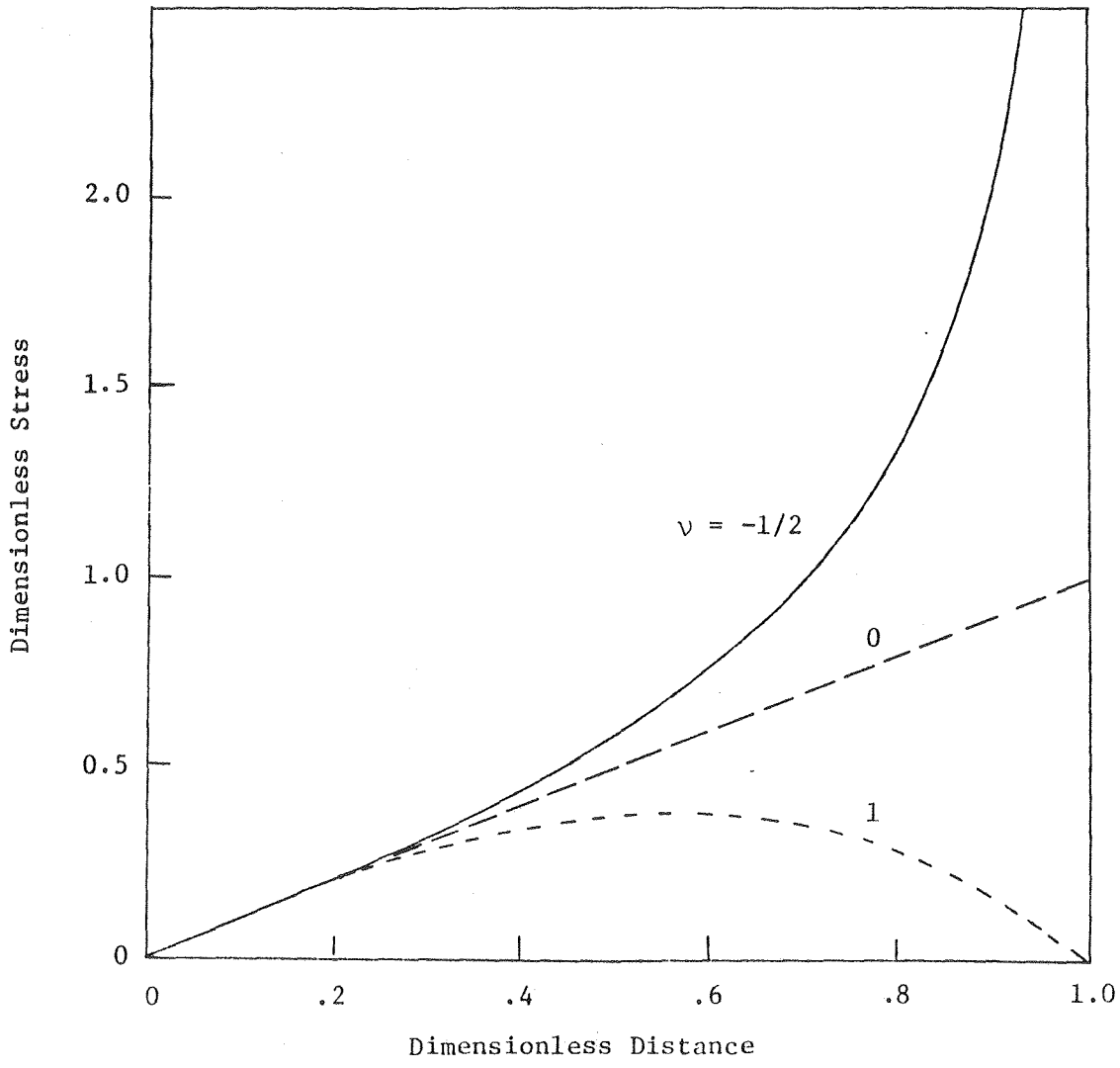
Dimensionless Stress
2.0
1.5
1.0
0.5
0
ν = -1/2
0
1
0
.2
.4
.6
.8
1.0
Dimensionless Distance

XBL 814-2898

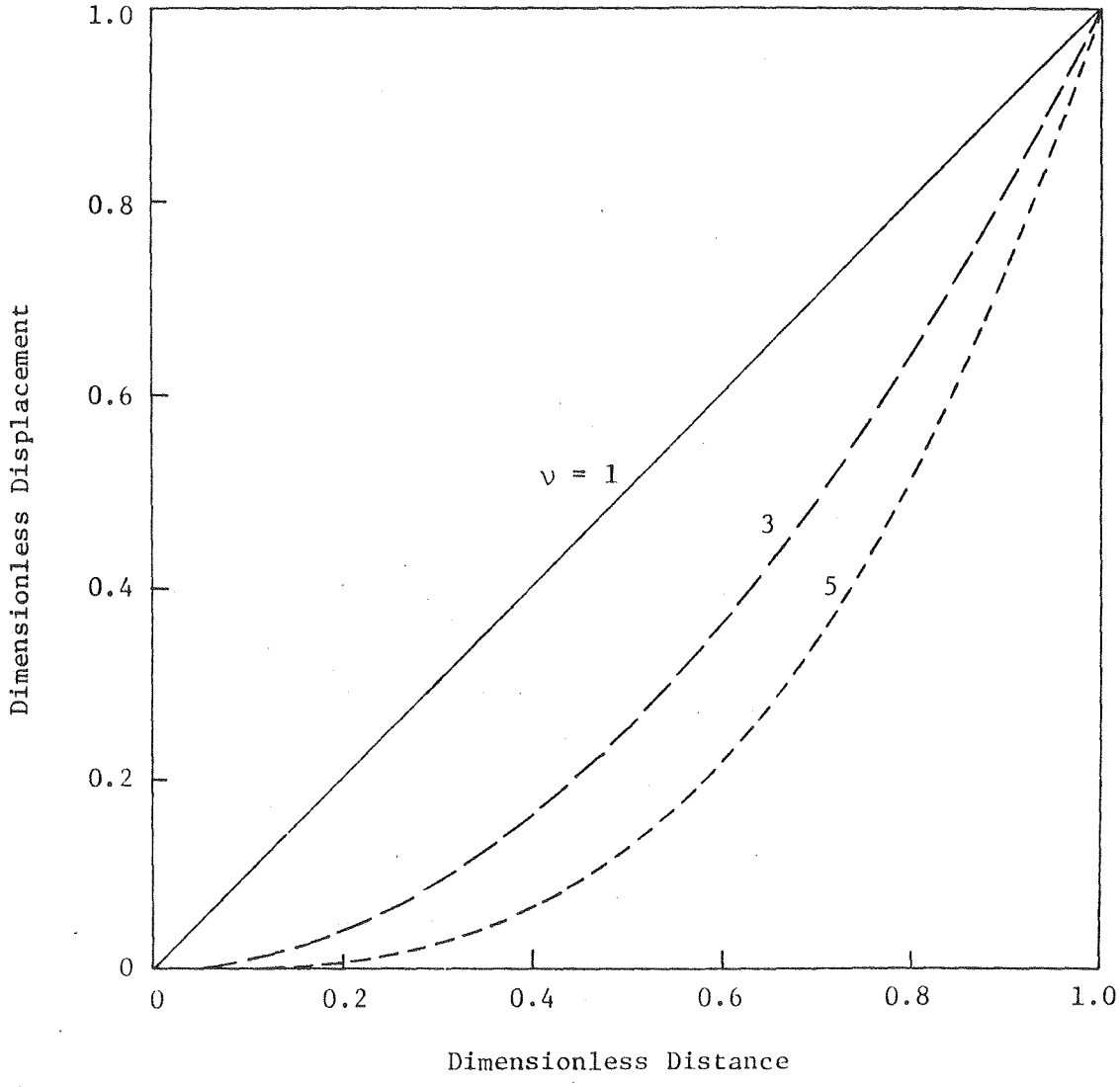
1.0
0.8
0.6
0.4
0.2
0
0
0.2
0.4
0.6
0.8
1.0
Dimensionless Displacement
Dimensionless Distance
ν = 1
3
5

XBL 814-2899

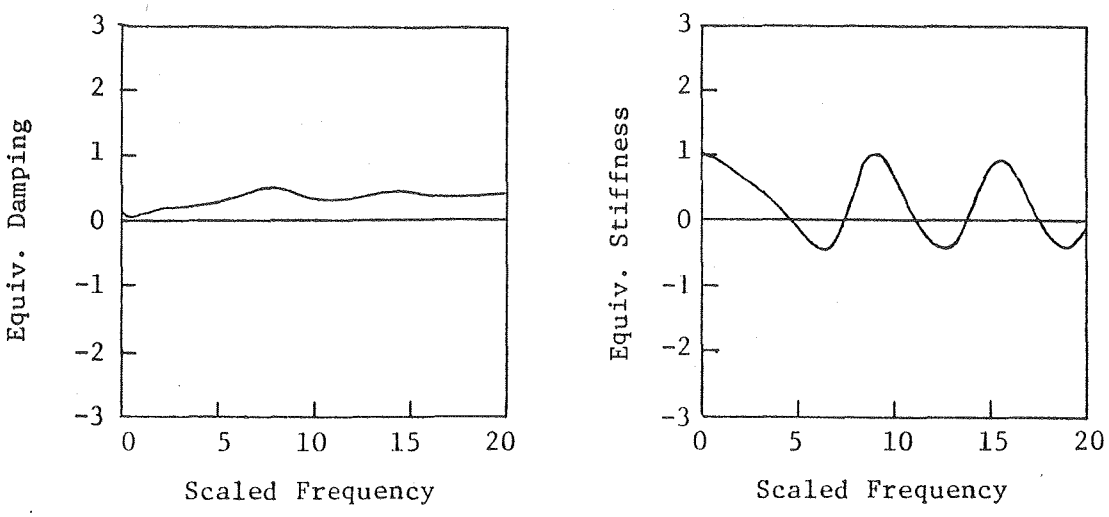
Equiv. Damping
3
2
1
0
-1
-2
-3
0
5
10
15
20
Scaled Frequency
Equiv. Stiffness
3
2
1
0
-1
-2
-3
0
5
10
15
20
Scaled Frequency

XBL 814-2900

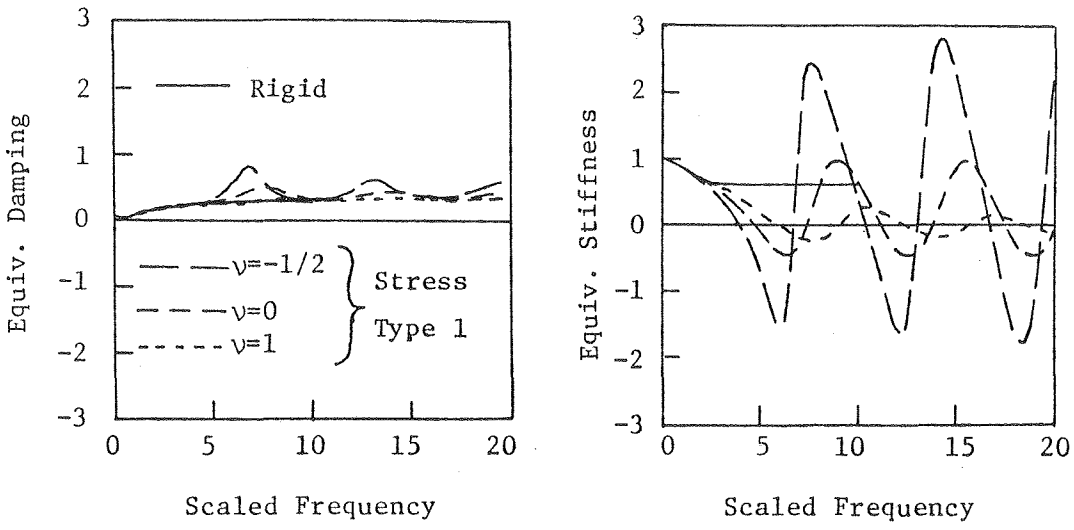
Equiv. Damping
Rigid
ν=-1/2
ν=0
ν=1
Stress
Type 1
Scaled Frequency
Equiv. Stiffness
Scaled Frequency

XBL 814-2901

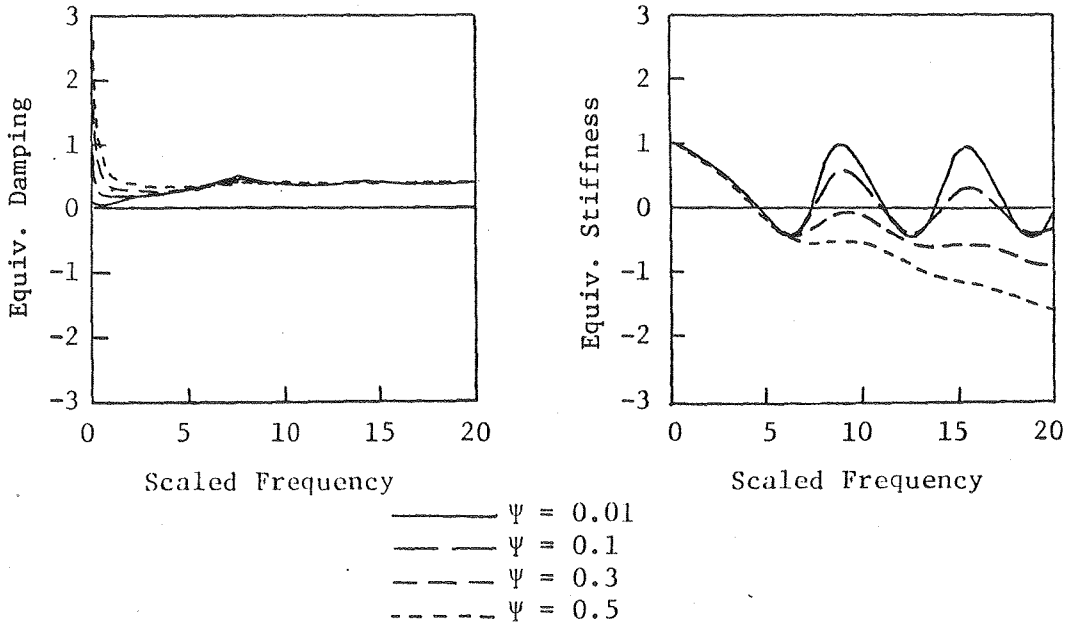
Equiv. Damping
3
2
1
0
-1
-2
-3
0
5
10
15
20
Scaled Frequency
Equiv. Stiffness
3
2
1
0
-1
-2
-3
0
5
10
15
20
Scaled Frequency
Ψ = 0.01
Ψ = 0.1
Ψ = 0.3
Ψ = 0.5

XBL814-2902

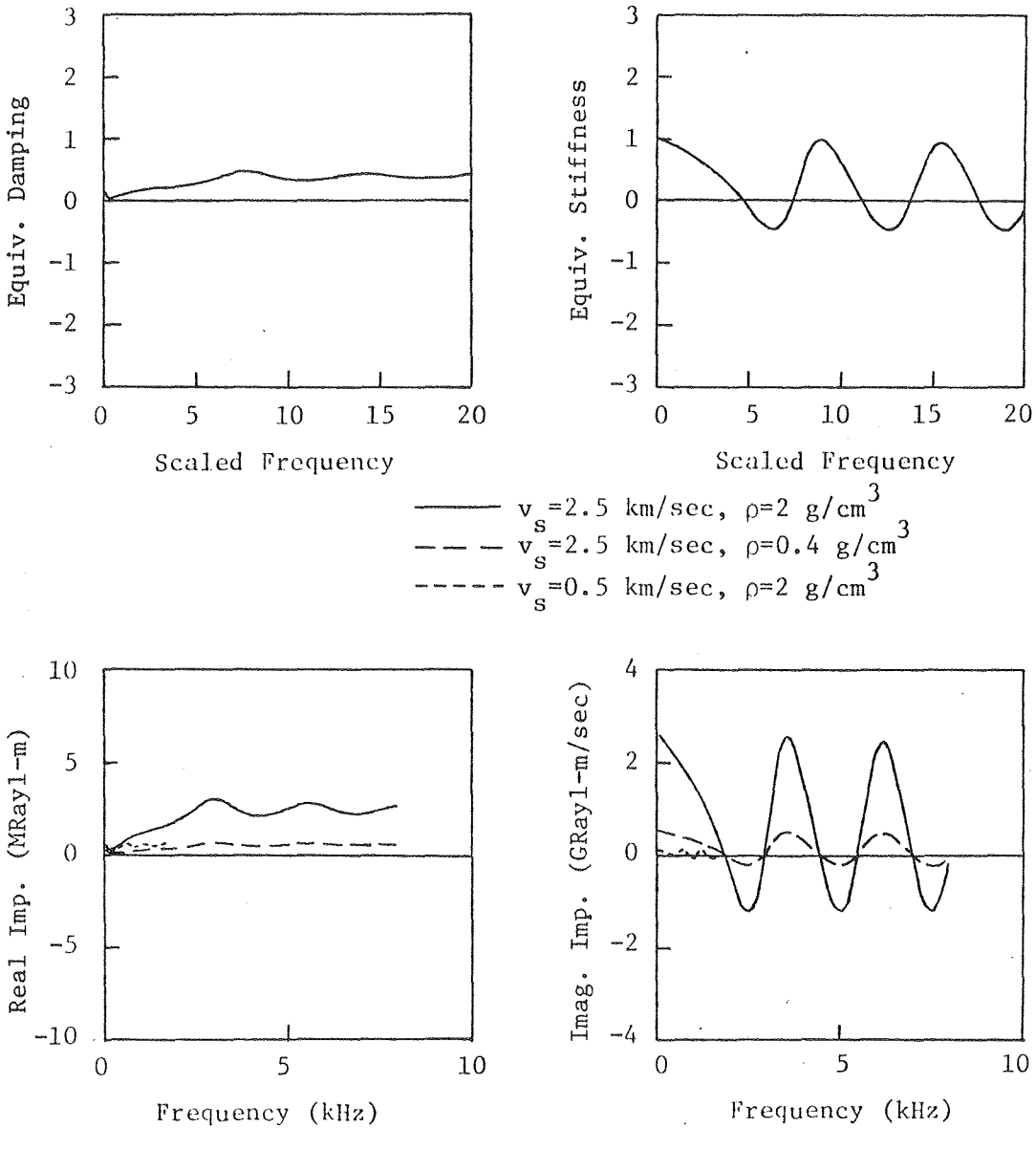
Equiv. Damping
Scaled Frequency
Equiv. Stiffness
Scaled Frequency
$v_s$=2.5 km/sec, ρ=2 g/cm$^3$
$v_s$=2.5 km/sec, ρ=0.4 g/cm$^3$
$v_s$=0.5 km/sec, ρ=2 g/cm$^3$
Real Imp. (MRayl-m)
Frequency (kHz)
Imag. Imp. (GRayl-m/sec)
Frequency (kHz)

XBL 814-2903

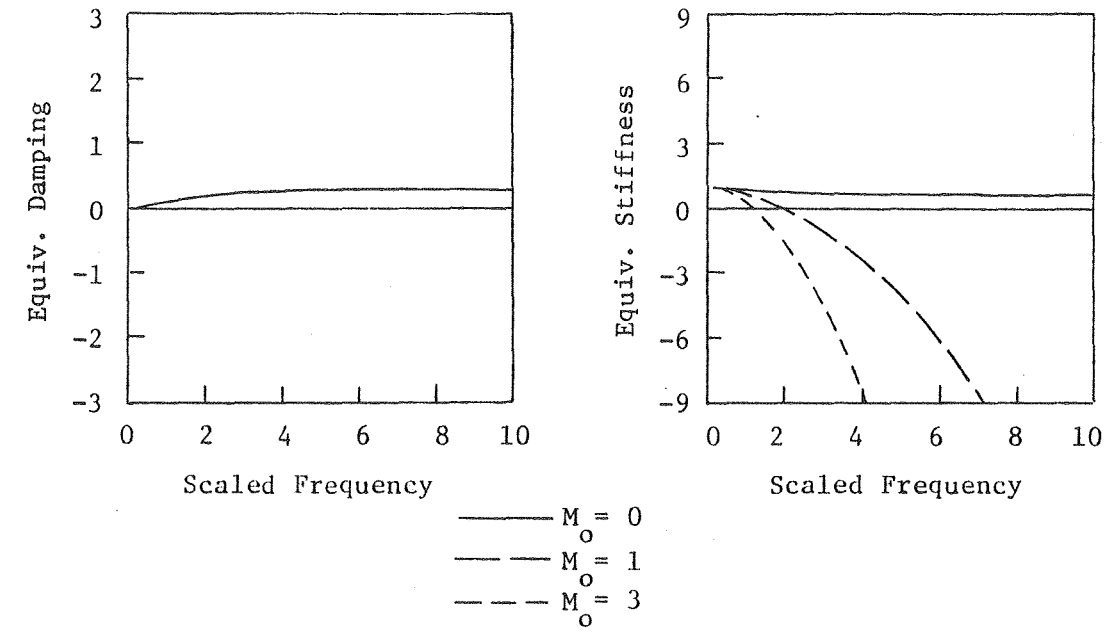
Equiv. Damping
3
2
1
0
-1
-2
-3
0
2
4
6
8
10
Scaled Frequency
Equiv. Stiffness
9
6
3
0
-3
-6
-9
0
2
4
6
8
10
Scaled Frequency
$M_o = 0$
$M_o = 1$
$M_o = 3$

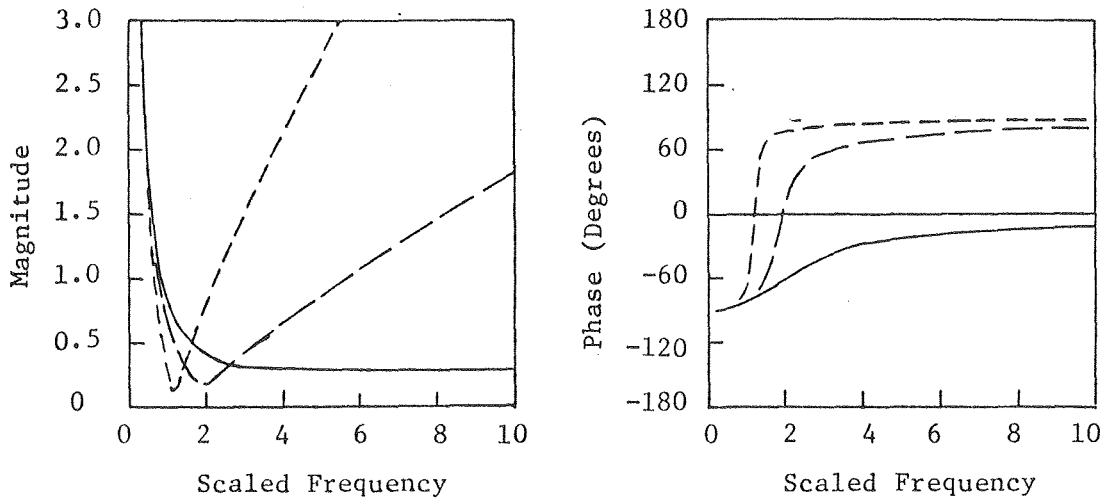
Magnitude
3.0
2.5
2.0
1.5
1.0
0.5
0
0
2
4
6
8
10
Scaled Frequency
Phase (Degrees)
180
120
60
0
-60
-120
-180
0
2
4
6
8
10
Scaled Frequency

XBL 814-2904

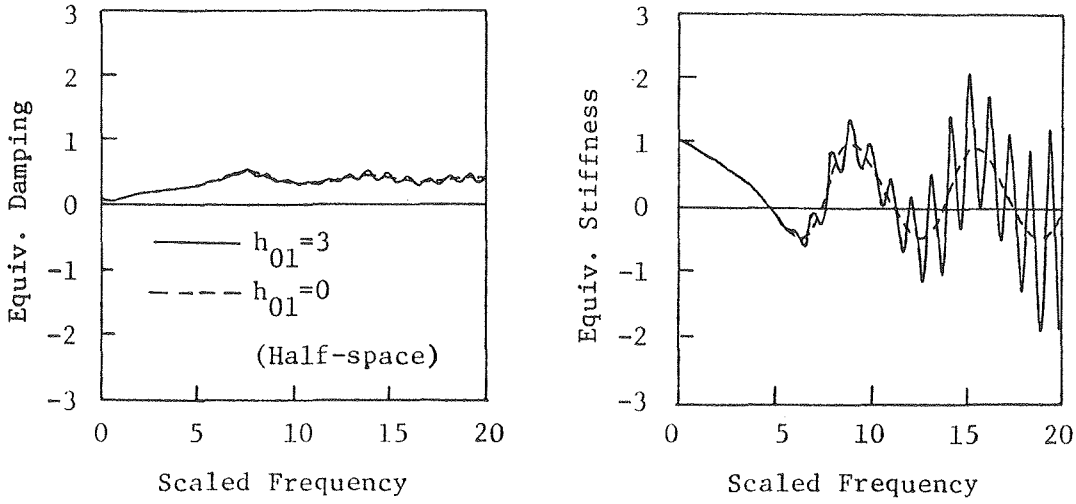
Equiv. Damping
3
2
1
0
-1
-2
-3
0
5
10
15
20
Scaled Frequency
$h_{01}$=3
$h_{01}$=0
(Half-space)
Equiv. Stiffness
3
2
1
0
-1
-2
-3
0
5
10
15
20
Scaled Frequency

XBL814-2905

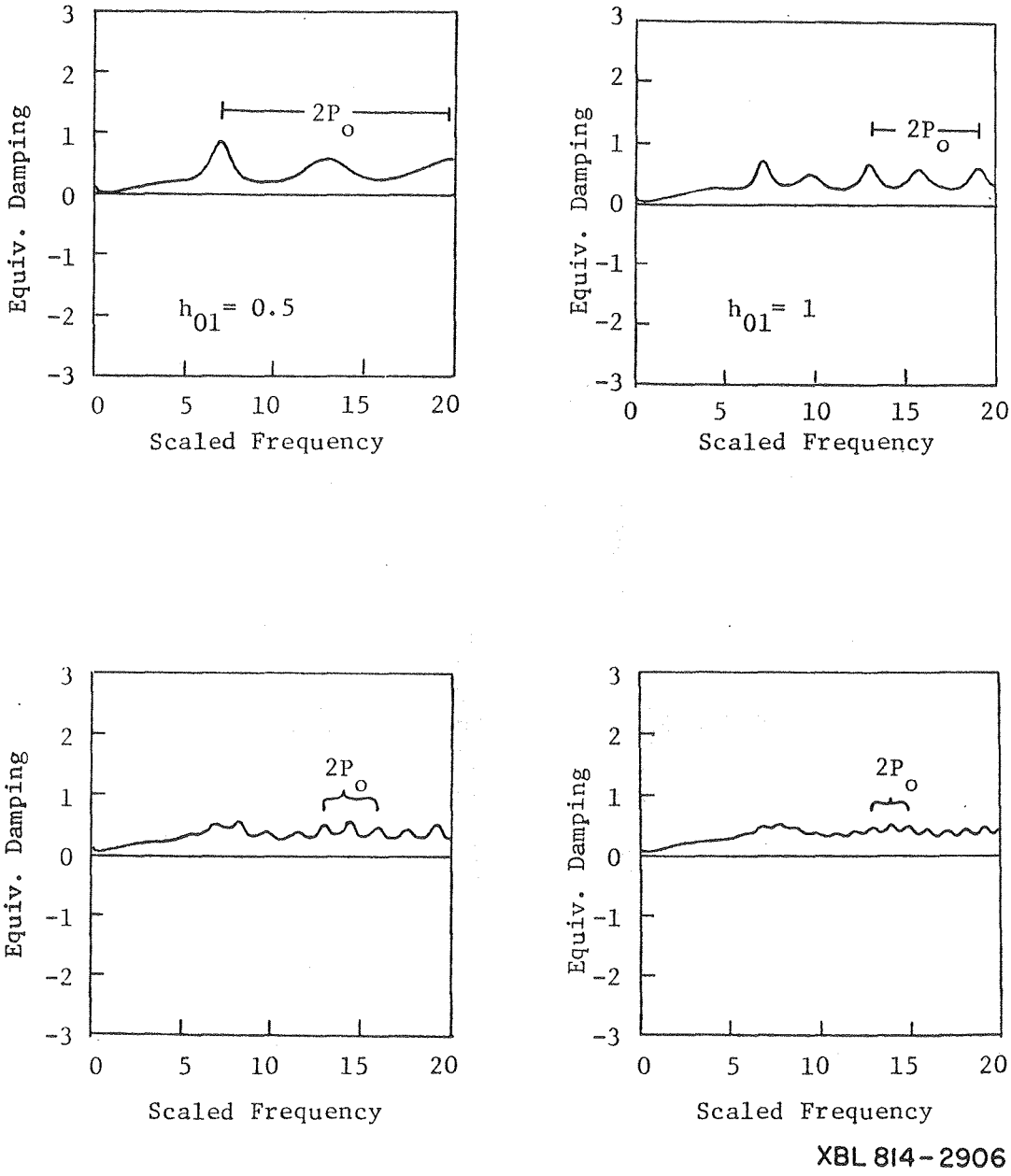
Equiv. Damping
Scaled Frequency
$2P_o$
$h_{01}$= 0.5
$h_{01}$= 1
3
2
1
0
-1
-2
-3
0
5
10
15
20

XBL 814-2906

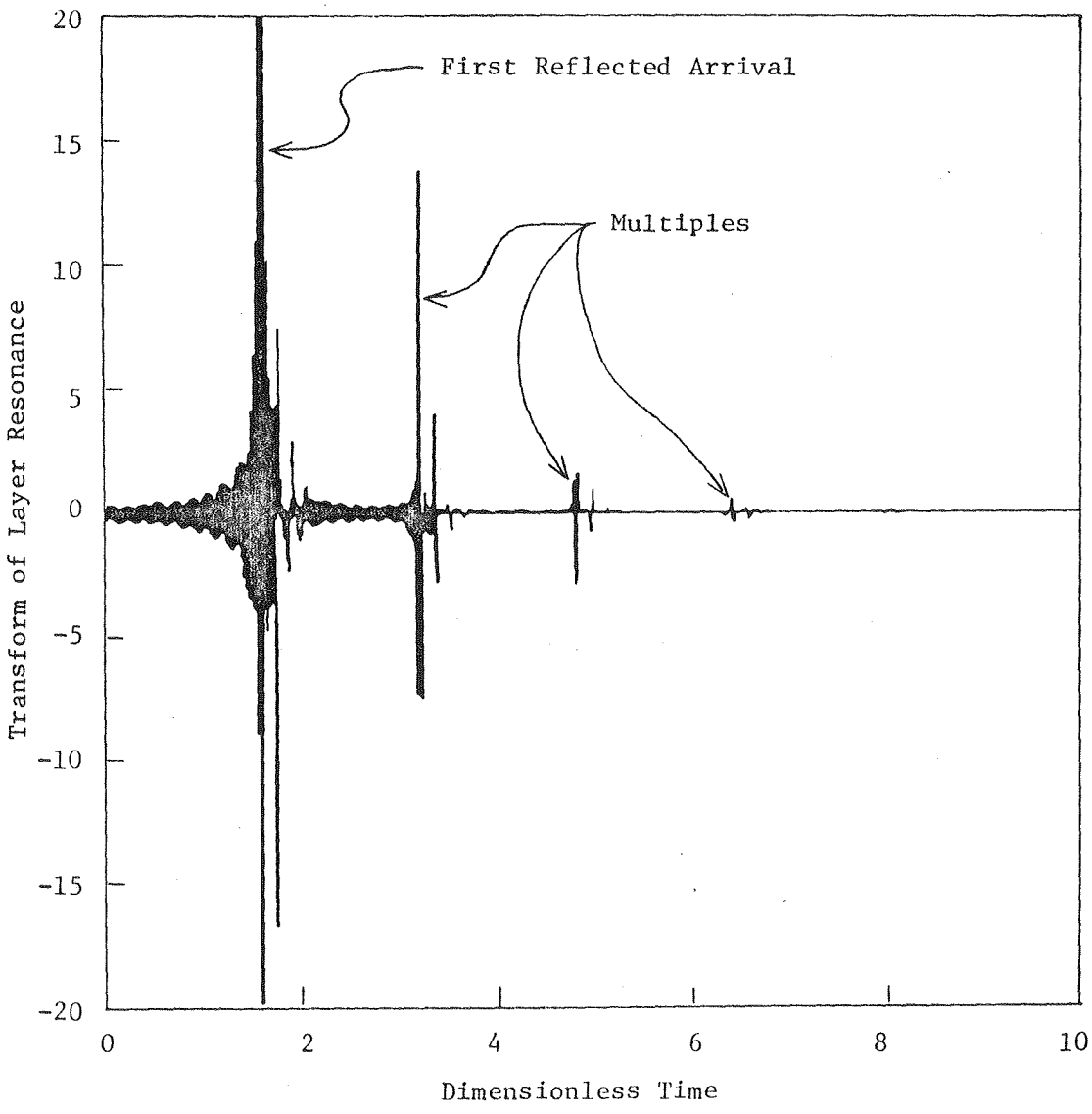
First Reflected Arrival
Multiples
Transform of Layer Resonance
20
15
10
5
0
-5
-10
-15
-20
0
2
4
6
8
10
Dimensionless Time

XBL 814-2907

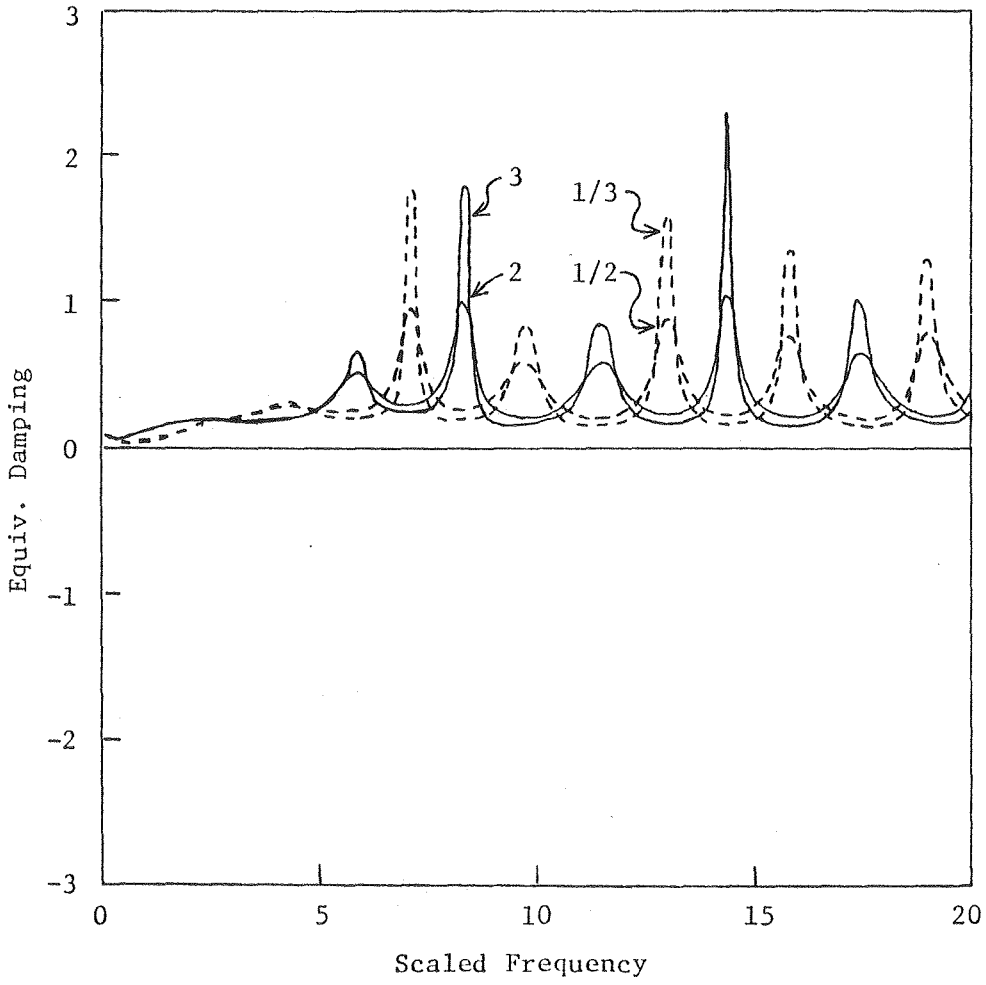


XBL 814-2908

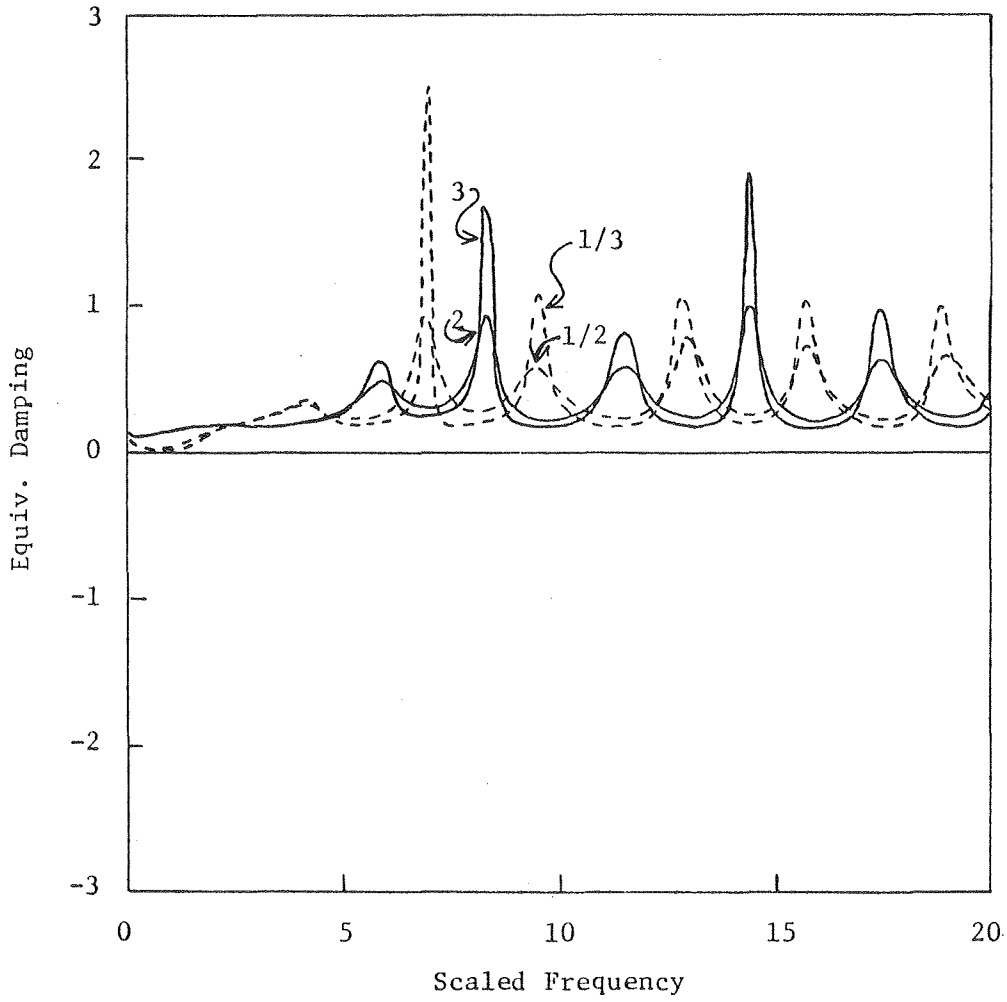


XBL 814-2909

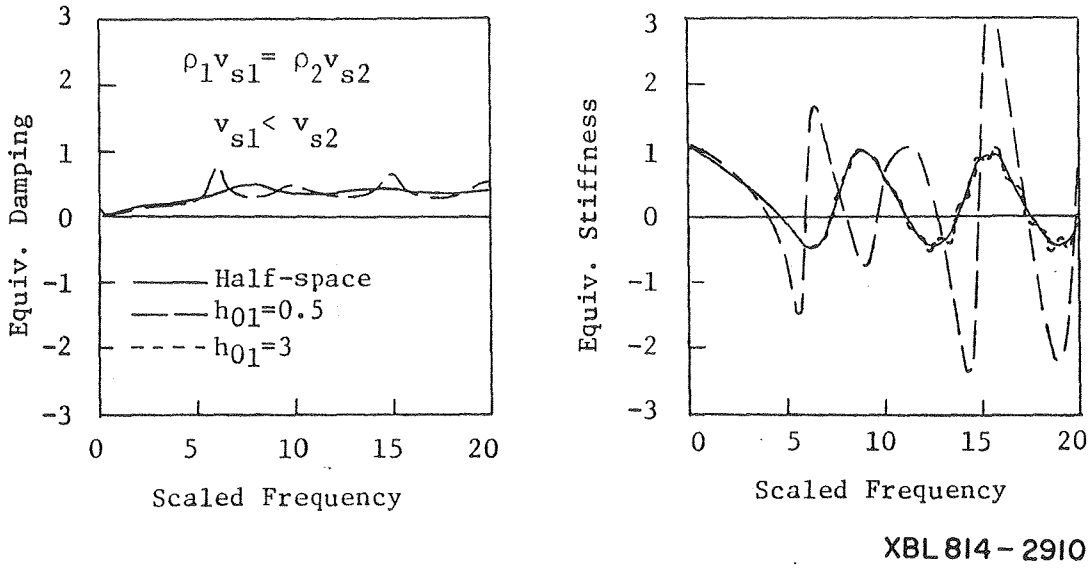
Equiv. Damping
3
2
1
0
-1
-2
-3
0
5
10
15
20
Scaled Frequency
$\rho_1 v_{s1} = \rho_2 v_{s2}$
$v_{s1} < v_{s2}$
Half-space
$h_{01}$=0.5
$h_{01}$=3
Equiv. Stiffness
3
2
1
0
-1
-2
-3
0
5
10
15
20
Scaled Frequency

XBL 814-2910

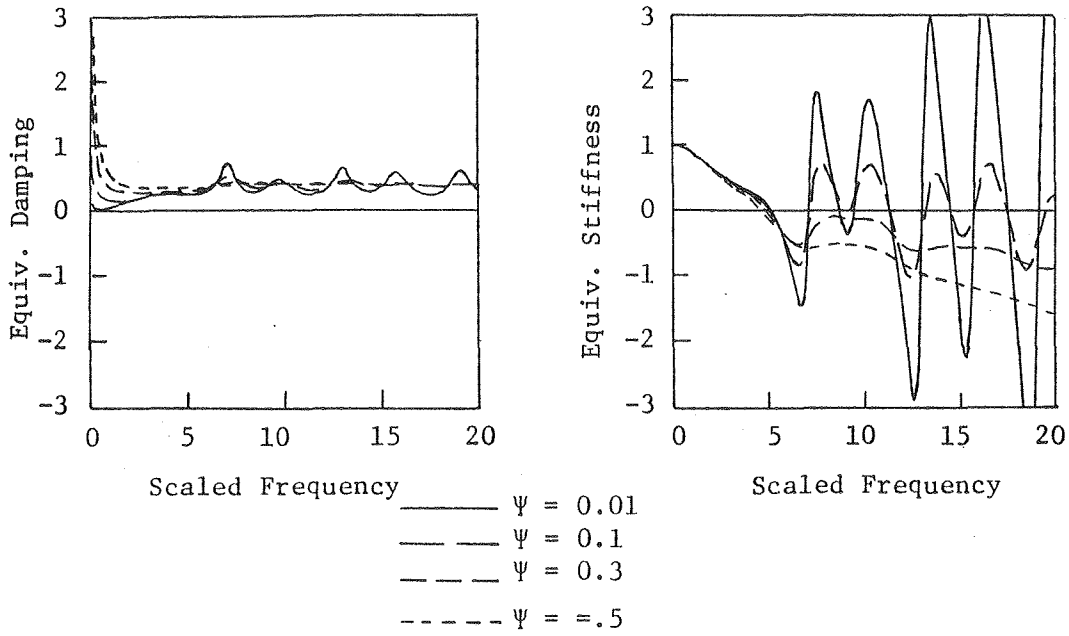
Equiv. Damping
3
2
1
0
-1
-2
-3
0
5
10
15
20
Scaled Frequency
Equiv. Stiffness
3
2
1
0
-1
-2
-3
0
5
10
15
20
Scaled Frequency
Ψ = 0.01
Ψ = 0.1
Ψ = 0.3
Ψ = =.5

XBL 814-2911

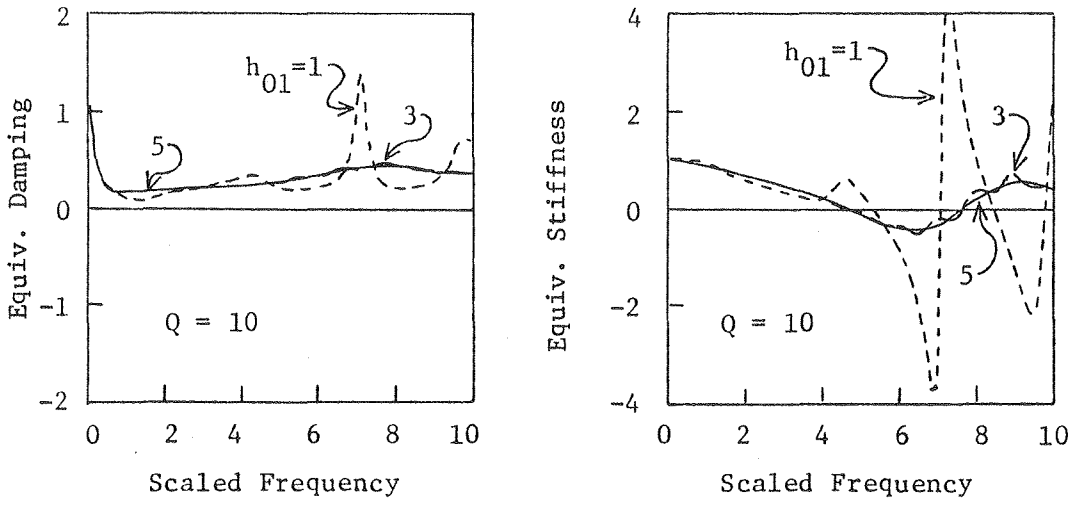
Equiv. Damping
2
1
0
-1
-2
$h_{01}$=1
3
5
Q = 10
0
2
4
6
8
10
Scaled Frequency
Equiv. Stiffness
4
2
0
-2
-4
$h_{01}$=1
3
5
Q = 10
0
2
4
6
8
10
Scaled Frequency

XBL 814-2912

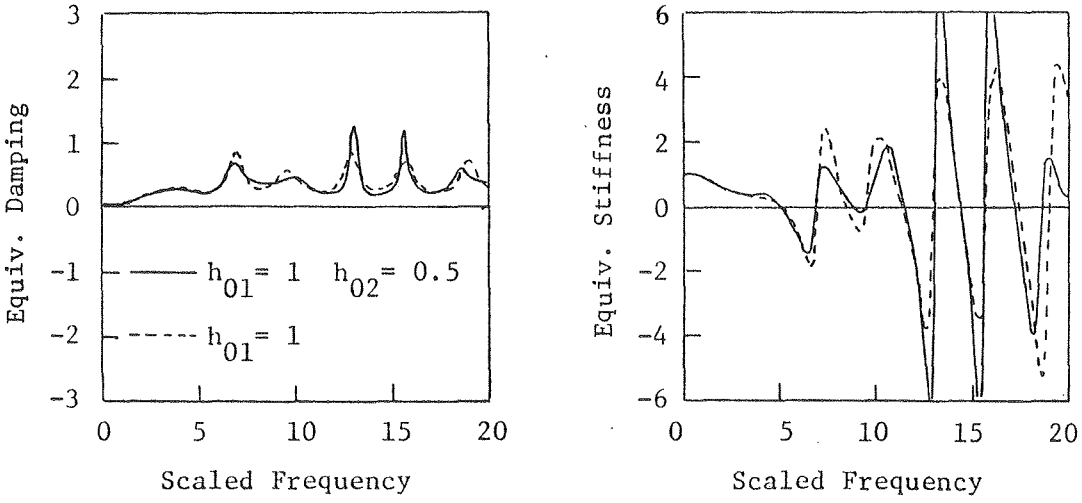
Equiv. Damping
3
2
1
0
-1
-2
-3
0
5
10
15
20
Scaled Frequency
$h_{01}$= 1 $h_{02}$= 0.5
$h_{01}$= 1
Equiv. Stiffness
6
4
2
0
-2
-4
-6
0
5
10
15
20
Scaled Frequency

XBL 814-2913